University of Crete

Physics Department

Master on Photonics and Nanoelectronics
Master Thesis

Part 1: Sensitive measurements of chirality with a cavity-based polarimeter

and

Part 2: Nanosecond-resolved magnetometry with spin polarized hydrogen atoms

By

Michail Xygkis

email: mixalis.xigis@gmail.com

Supervisor Prof.: Peter T. Rakitzis

Table of Contents

Abstract

This thesis is divided into two different parts. The first part focuses on chiral measurements using optical-cavity-enhanced polarimetry. Detecting and quantifying chirality plays a significant role in a variety of fields ranging from analytical and biological chemistry to pharmacology and fundamental physics. Potential applications of chiral sensing include drug design and synthesis, protein structure determination, and the study of parity non-conservation in select atomic/molecular transitions, which is a symmetry-breaking effect owing to the weak force, manifesting as optical activity. In the present study, the chirality of gases and biological liquid solutions was measured via our cavity-enhanced methods polarimetry. The basic idea behind the technique is that the weakly rotating samples are placed in a high-finesse optical cavity and, through multiple cavity passes, the amplification of the weak polarimetric signal is achieved. The second part focuses on magnetometry. Magnetometers have a wide variety of applications, including magnetic navigation, magnetic anomaly detection, current sensing, the measurement of biological magnetic fields, and much more. Conventional atomic magnetometers can typically operate down to the millisecond or sub-millisecond timescale. However, there are applications that require nanosecond or picosecond time resolution, such as the measurement of surface magnetism, and the ultrafast generation of magnetic fields with short-pulse lasers, with applications in laser fusion, particle-beam generation, and laboratory astrophysics. In this part of the thesis we investigate a novel low-cost, high-sensitivity technique for measuring magnetic fields with nanosecond time response, by detecting the

hyperfine oscillation of an appropriately produced macroscopic time-depended polarization of electronic spins in the presence of a static or time-dependent magnetic field.

List of Abbreviations and Symbols

LASER: Light Amplification by Stimulated Emission of Radiation

RCPL: Right Circularly Polarized Light

LCPL: Left Circularly Polarized Light

LPL: Linear Polarized Light

PCRDP: Pulsed Cavity Ring Down Polarimetry

CW: Clock Wise

CCW: Counter Clock Wise

SPA: Spin Polarized Atoms

SPD: Spin Polarized Deuterium

SPH: Spin Polarized Hydrogen

SERF: Spin Exchange Relaxation Free

SQUID: Superconductive Quantum Integrated Devices

NPI-OR: Non-Planarity Induces Optical Rotation

EMF: Electro-Magnetic Force

Part 1: Ultra-Chiral Measurements

In this chapter, light and its “classical” properties will be presented, as well as the importance and basic principles of a Laser. More specifically, the basic equation,that describes light as a transverse electromagnetic wave is derived from Maxwell equations. In addition, we will introduce the concept

of birefringence, the mathematical tools to describe it and the most common sources of birefringence that exist in a cavity. Then, a novel technique that enables to measure the optical activity of the null sample without the need to remove the sample to measure the background and cancel out spurious birefringence is exhibited. Finally, the experimental results will be displayed and discussed.

1.1 Description of Light and Laser

Light, viewed classically, is a transverse electromagnetic wave. This electromagnetic wave consists of an oscillation electric and a magnetic field perpendicular to each other. By convention, the polarization of electromagnetic waves refers to the direction of the oscillation of the electric field. This is in contrast to longitudinal waves, such as sound waves, in which the oscillation is confined to the direction of propagation. Most light sources in nature emit unpolarized light i.e. light consisting of many wave trains whose directions of oscillation are completely random. On the other hand, a laser (acronym for "Light Amplification by Stimulated Emission of Radiation"), differs from other light sources. Laser emits light coherently, spatially and temporally. This is a very important characteristic of laser light, because due to the spatial coherence it is possible to focus the emitted light to a tight spot, which enables applications such as laser cutting and lithography. In addition, spatial coherence allows a laser beam to stay narrow, over great distances, which enables applications such as laser pointers. Regarding the temporal coherence, this allows the laser light to have a very narrow spectrum i.e. the laser light is almost monochromatic. Temporal coherence enables the creation of ultrashort laser pulses, which reach the femtoseconds scale.

Each laser system has two essential components: a laser cavity which traps light and supplies the needed optical feedback, and a gain medium that amplifies light in the presence of an external pump. The most common and primary laser cavities are of Fabry-Perot type, (see Fig. (1)). In this type of laser cavities, light undergoes multiple reflections between two high-reflectivity mirrors.

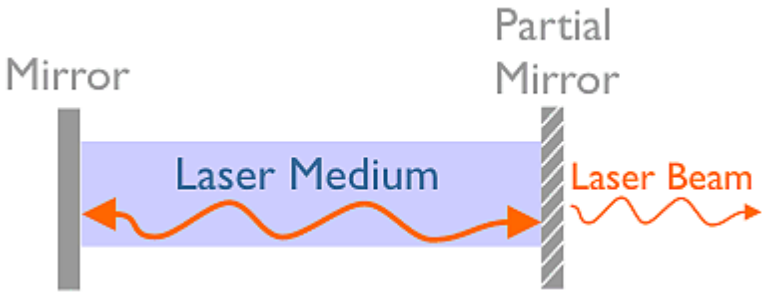

Figure 1 : Representation of a Fabry-Perot laser cavity

To describe an electromagnetic wave, we need two field-intensity vectors, E and HE, which are related to each other by:

$$\nabla \times H = J + \varepsilon_o \frac{\partial E}{\partial t} + \frac{\partial P}{\partial t} \quad (1)$$

$$\nabla \times E = \mu_o \frac{\partial H}{\partial t} \quad (2)$$

Where, E is the electric field, H is the magnetic Field, J is the current and P is the polarization current induced by the electric field (a term of the form $\frac{\partial m}{\partial t}$ can be added to (2) but will be ignored for these calculations).
In free space, the conduction current J is zero. If we take the curl of (2) and eliminate H, using of (1) we obtain:

$$\nabla \times \nabla \times E = \mu_o \frac{\partial}{\partial t}(\nabla \times H) + \frac{\partial P}{\partial t} = \varepsilon_o \mu_o \frac{\partial^2}{\partial t^2} E \quad (3)$$

or

$$\nabla^2 E - \frac{1}{c^2} \frac{\partial^2}{\partial t^2} E = 0$$

Where, $\frac{1}{c^2} = \varepsilon_o \mu_o$ is the square of the velocity of light. If the procedure is reversed to eliminate E, we obtain the same equation with H substituted for E in (3):

$$\nabla^2 H - \frac{1}{c^2} \frac{\partial^2}{\partial t^2} H = 0 \quad (4)$$

From Maxwell's equations we derive the wave equation. Therefore, we prove that any function of the form f(t-$\hat{a}_n\vec{r}$/c) is a solution, whereas is a unit vector. It is easy to show this in one dimension and only slightly more complicated to do so for the general case. Physically, it merely means that the wave propagates in the direction of $\hat{a}_n$ with a velocity c. If for simplicity we assume the propagation of the wave in z direction, the solutions of (3), (4) and take into account H=$\frac{1}{\mu o}$B, resulting in:

$$E = \overrightarrow{E_o}e^{-i(\vec{k}\hat{z}-\omega t)}, B = \overrightarrow{B_o}e^{-i(\vec{k}\hat{z}-\omega t)} \quad (5)$$

Here, $\overrightarrow{E_o}$ and $\overrightarrow{B_o}$ are called the polarization vectors for the electric and magnetic fields. These are complex 3-dimensional vectors. The wave vector $\vec{k}$ and angular frequency ω are real and are related by ω = c/$\vec{k}$. This relation implies that electromagnetic waves are dispersionless with velocity c: the speed of light.

In addition, we find that for plane waves:

$$\overrightarrow{B_o} = \frac{(\vec{k}x\overrightarrow{E_o})}{\omega} \quad (6)$$

This equation implies that the magnetic field in a plane wave is completely determined by the electric field. In particular, it implies that their magnitudes are related by:

$$|\overrightarrow{E_o}| = c\overrightarrow{B_o} and \vec{k} * \overrightarrow{E_o} = 0, \vec{k} * \overrightarrow{B_o} = 0, \overrightarrow{B_o} * \overrightarrow{E_o} = 0 \quad (7)$$

In other words, the polarization vector of the electric field, the polarization vector of the magnetic field, and the direction $\vec{k}$,where the plane wave is propagating are all orthogonal.

Since $\overrightarrow{E_o}$ is orthogonal to $\vec{k}$ we can also write $\overrightarrow{E_o} = (E_x, E_y, 0)$with Ex and E_y complex numbers.

The two complex amplitudes E_x and E_y each have magnitudes and phases.

We can write these explicitly as $E_x = |E_x|e^{i\varphi_x}$ Ex and $E_y = |E_y|e^{i\varphi_y}$.

So, one would need four real numbers to specify the polarization vector. We usually aggregate the phases into an overall phase and the difference in phase between E_x and E_y, $\varphi = \varphi_x - \varphi_y$. The reason for doing this is that as t and z change, the phases of E_x and E_y change in the same way, while ϕ is unaffected. We don't usually care about this overall phase, or about the

overall magnitude $E = |E_x|^2 + |E_y|^2$. Thus, to specify a polarization vector, we talk about the relative size of E_x and E_y and the phase difference $\varphi = \varphi_x - \varphi_y$. Thus, the most general formula is:

$$E = E_x\hat{x}\cos(kz - \omega t + \varphi_x) + E_y\hat{y}\sin\left(kz - \omega t + \varphi_y\right) \qquad (8)$$

Linear polarization

A plane wave is termed linearly polarized if there is no phase difference between $E_x$and E_y.We can write linear polarizations as $\overrightarrow{E_o}$=(E_x, E_y,0) and choose the overall phase so that E_x and E_y are real numbers. If E_y =0 but $E_x \neq 0$, we have $\vec{E} = \hat{x}E_o e^{-i(\vec{k}\hat{z}-\omega t)}$. In addition, from equation (6), we have:

$\vec{B} = \frac{-1}{c}E_o e^{-i(\vec{k}\hat{z}-\omega t)}$.

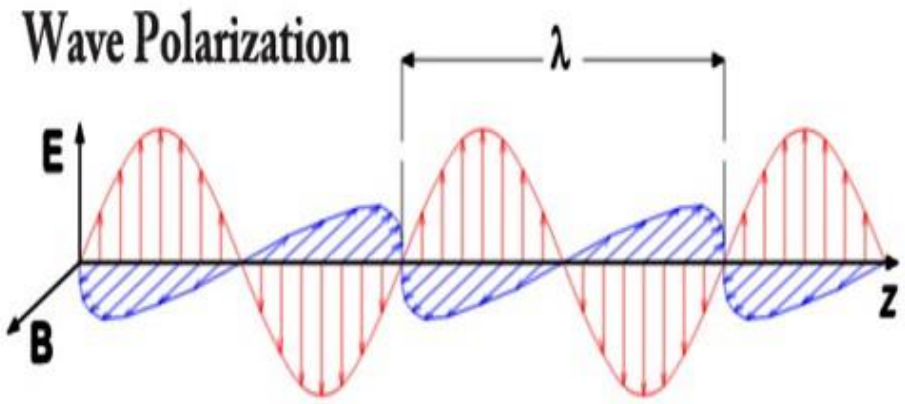

Figure 2- Linear polarized light in x-y plane with z direction propagation

Circular polarization

What if the components of the electric field are not in phase? First suppose they have the same magnitude but are a quarter wavelength out of phase, so $\varphi_x - \varphi_y = \pi/2$. Then,$\overrightarrow{E_o}$=(E_o, $e^{i\frac{\pi}{2}}E_o$, 0), =(E_o,iE_o, 0). Thus, $\vec{E}$=($E_o e^{-i(\vec{k}\hat{z}-\omega t)}$,i$E_o e^{-i(\vec{k}\hat{z}-\omega t)}$,0). This is called left-handed circularly polarized light. The wave is propagating at z direction and, as time progresses, polarization also rotates in the x-y plane.

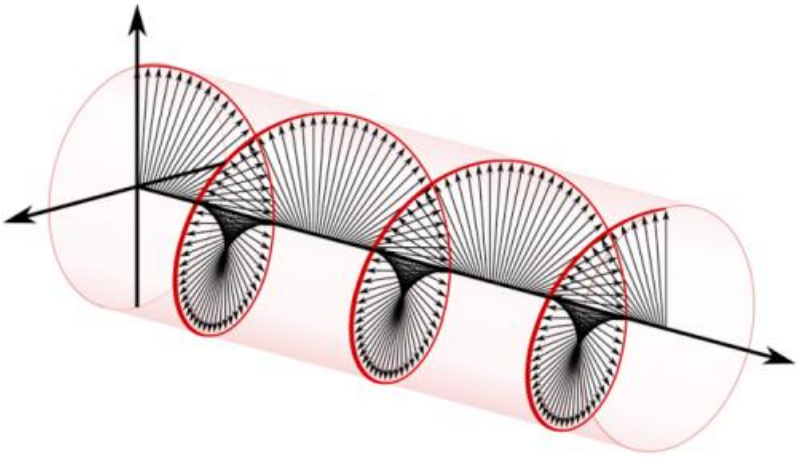

Figure 3-Left Circularly polarized light changes the direction of its polarization as it propagates.

Similarly, taking $\varphi_x - \varphi_y = -\pi/2$, we have $\overrightarrow{E_o}$=(E_o, $e^{-i\frac{\pi}{2}}E_o$, 0), = (E_o, -iE_o, 0). Thus, $\overrightarrow{E}$=($E_o e^{-i(\vec{k}\hat{z}-\omega t)}$, -i$E_o e^{-i(\vec{k}\hat{z}-\omega t)}$,0) which is called right circular polarized light.

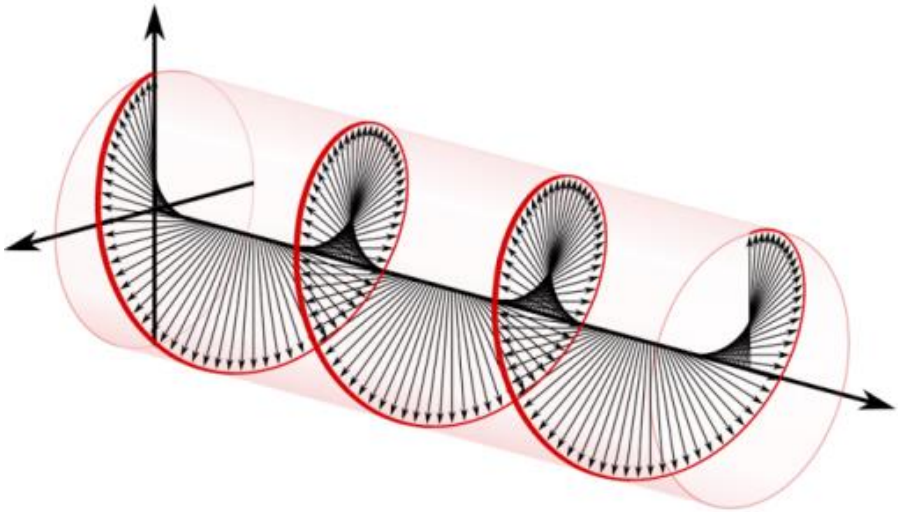

Figure 4- Right Circularly polarized light changes the direction of its polarization as it propagates.

1.2 Birefringence

Birefringence is the optical property of a material having a refractive index that depends on the polarization and propagation direction of light.[1] These optically anisotropic materials are said to be birefringent (or birefractive). Birefringence is often quantified as the maximum difference between refractive indices exhibited by the material. Crystals with non-cubic crystal structures are often birefringent, as are plastics under mechanical stress. Birefringence is responsible for the phenomenon of double refraction whereby a ray of light, when incident upon a birefringent material, is split by polarization into two rays taking slightly different paths.

In an isotropic medium (including free space) the so-called electric displacement $\vec{D}$ is just proportional to the electric field $\vec{E}$ according to $\vec{D} = \varepsilon\vec{E}$ where the material's permittivity ε is just a scalar (and equal to $n^2=\varepsilon_0$ where n is the index of refraction). However, in an anisotropic material exhibiting birefringence, the relationship between D and E must now be described using a tensor equation:

$$\vec{D} = \breve{\varepsilon}\vec{E} \tag{9}$$

where ε is now a 3 × 3 permittivity tensor and now $\vec{D}$ is not proportional to $\vec{E}$. More precisely,

$$D_i = \varepsilon_o \sum_{j=1}^{3} \varepsilon_{ij} E_j \equiv \varepsilon_o \varepsilon_{ij} E_j \tag{10}$$

Or equivalently

$$\begin{pmatrix} E_1 \\ E_2 \\ E_3 \end{pmatrix} = \frac{1}{\varepsilon_o} \begin{pmatrix} \varepsilon_{11}^{-1} & \varepsilon_{12}^{-1} & \varepsilon_{13}^{-1} \\ \varepsilon_{21}^{-1} & \varepsilon_{22}^{-1} & \varepsilon_{23}^{-1} \\ \varepsilon_{31}^{-1} & \varepsilon_{32}^{-1} & \varepsilon_{33}^{-1} \end{pmatrix} \begin{pmatrix} D_1 \\ D_2 \\ D_3 \end{pmatrix} \tag{11}$$

Now, we define the magnitude we : density of energy as :

$$w_e \equiv \frac{1}{2}\vec{D}\vec{E} = \frac{1}{2}\varepsilon_{ij}E_iE_j = \frac{1}{2\varepsilon_o\varepsilon_{ij}} D_iD_j = constant \tag{12}$$

Taking into account , and defining x≡$\frac{D_1}{\sqrt{2\varepsilon_o w_e}}$,y≡$\frac{D_2}{\sqrt{2\varepsilon_o w_e}}$,z≡$\frac{D_3}{\sqrt{2\varepsilon_o w_e}}$, we obtain :$\frac{x^2}{n_x^2}+\frac{y^2}{n_y^2}+\frac{z^2}{n_z^2}=1$, which is an elliptical equation.

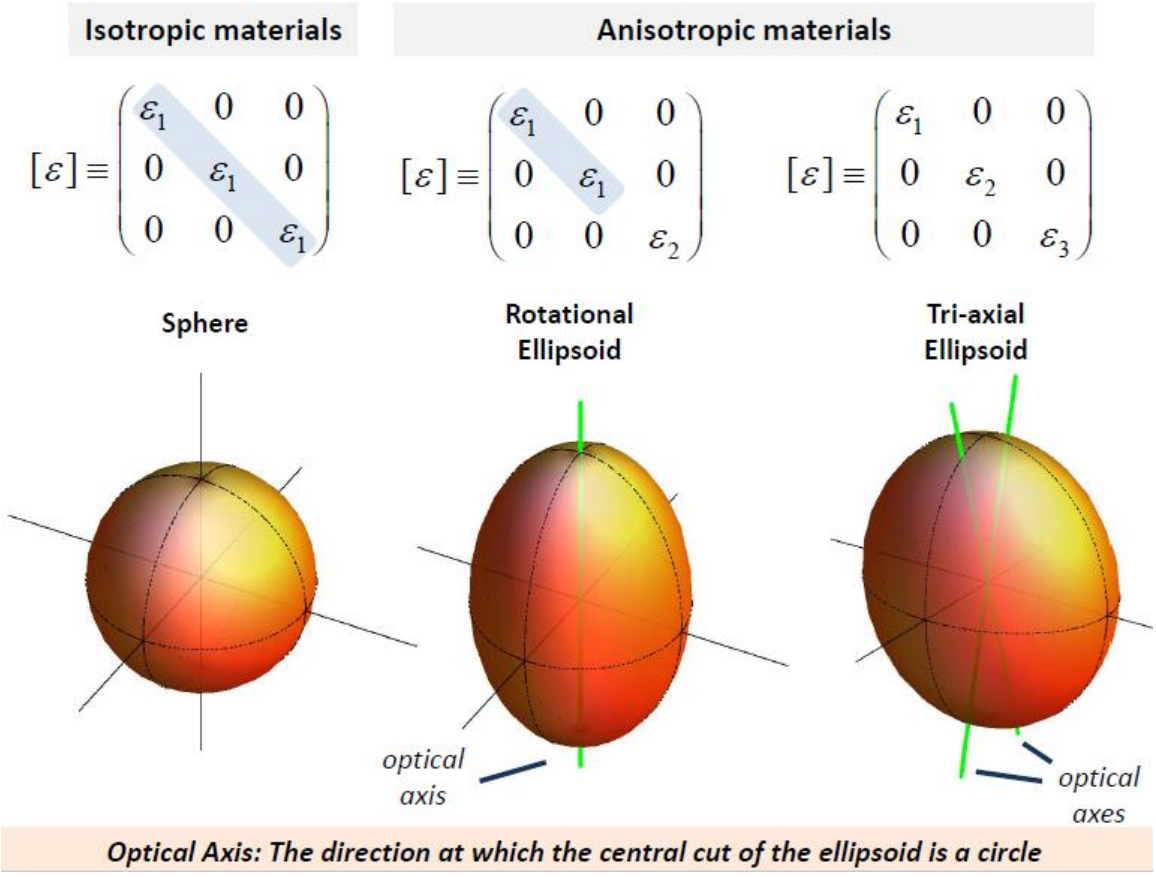

Figure 5-Isotropic and anisotropic materials

The simplest type of birefringence is described as uniaxial, meaning that there is a single direction governing the optical anisotropy whereas all directions perpendicular to it (or at a given angle to it) are optically equivalent. Thus, rotating the material around this axis does not change its optical behavior. This special direction is known as the optic axis of the material. Light propagating parallel to the optic axis (whose polarization is always perpendicular to the optic axis) is governed by a refractive index n_o (for "ordinary") regardless of its specific polarization. For rays with any other propagation direction, there is one linear polarization that would be perpendicular to the optic axis, and a ray with that polarization is called an ordinary ray and is governed by the same refractive index value n_o. However, for a ray propagating in the same direction but with a

polarization perpendicular to that of the ordinary ray, the polarization direction will be partly in the direction of the optic axis, and this extraordinary ray will be governed by a different, direction-dependent refractive index. Because the index of refraction depends on the polarization, when unpolarized light enters a uniaxial birefringent material, it is split into two beams travelling in different directions, one having the polarization of the ordinary ray and the other the polarization of the extraordinary ray. The ordinary ray will always experience a refractive index n_o of whereas the refractive index of the extraordinary ray will be in between n_o and n_e, depending on the ray direction as described by the index ellipsoid. The magnitude of the difference is quantified by the birefringence:

$$\Delta \mathrm{n} = n_e - n_o \tag{13}$$

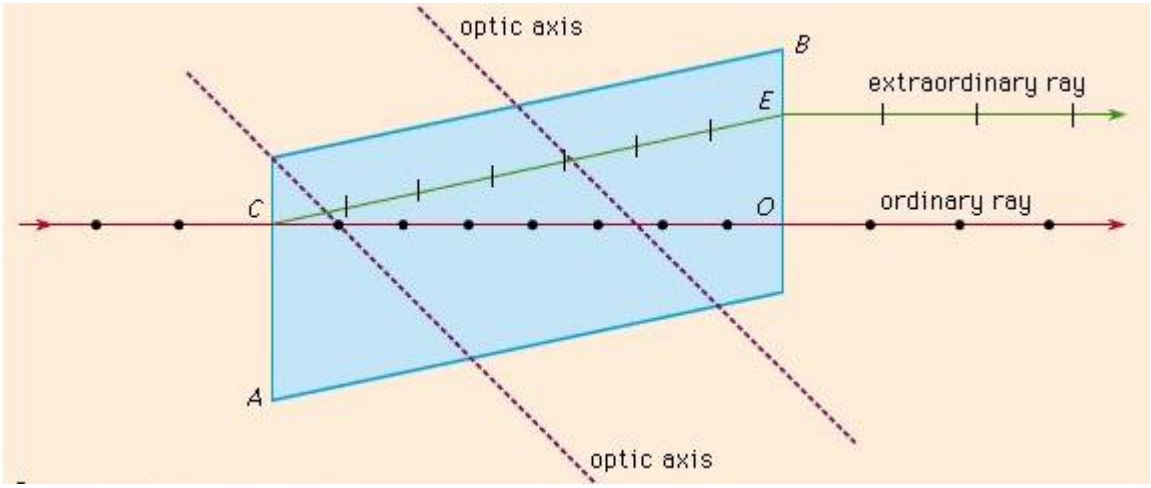

Figure 6-Incoming light in the parallel (p) polarization sees a different effective index of refraction than light in the perpendicular (s) polarization, and is thus refracted at a different angle

1.2.2 Circular Birefringence:

If a plane polarized beam propagates down the optic axis of a material exhibiting circular birefringence it is resolved into two collinear circularly polarized beams, each propagating with a slightly different velocity ($n_+ \neq n_-$). When these two components emerge from the material, they recombine into a plane polarized beam whose plane of polarization is rotated from that of the incident beam. This effect of producing a

progressive rotation of the plane of polarization with path length is called optical activity, and is used to produce optical rotators.

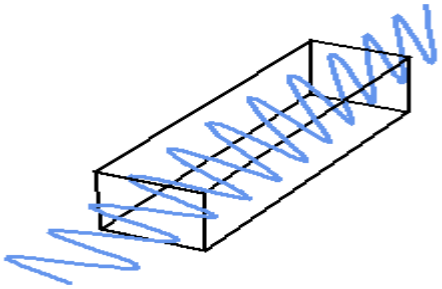

Figure 7- Anisotropic material induce circular Birefringence ($n_+ \neq n_-$).

1.2.1 Linear Birefringence

Linearly birefringent uniaxial crystalline materials are characterized by having a unique axis of symmetry, called the optic axis, which imposes constraints upon the propagation of light beams within the crystal. Two modes are permitted, either as an ordinary beam polarized in a plane normal to the optic axis, or as an extraordinary beam polarized in a plane containing the optic axis. Each of the beams has an associated refractive index, such that both the electric field (wave normal) velocities and the beam (ray) angles of refraction are different. That way, this kind of materials transform linear polarized light to elliptical then to circular again to elliptical and again to linear etc.

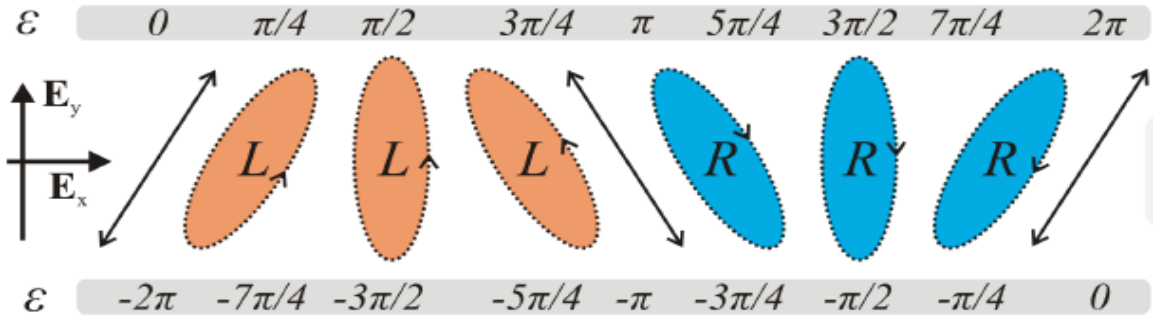

Figure 8-Polarization as a function of the relative phase between the two components E_x , E_y.

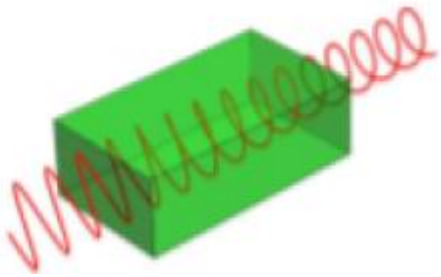

Figure 9- Anisotropic material induce linear Birefringence ($n_x \neq n_y$).

1.2.3 Sources of Birefringence

There are many different sources of optical birefringence in a real experiment. The most common sources that are existed in a cavity are:

- Stress birefringence results when isotropic materials are stressed or deformed (i.e., stretched or bent) causing a loss of physical isotropy and consequently a loss of isotropy in the material's permittivity tensor
- Circular birefringence, as it is mentioned before, in gasses, liquid solutions and from solid materials which have different refractive index from the right and left circular component of the incident light beam.
- Faraday effect, showed that linearly polarized light would undergo a rotation of the plane of polarization upon being transmitted through a medium that has a magnetic field applied along the direction of propagation. Therefore, a longitudinal magnetic field results in the medium becoming optically active[2]. In its simplest form the rotation, φ, is proportional to the strength of the magnetic field, B, and the length of the sample, l as expressed in Eq. 14:

$$\phi = V \int_0^l B dl = VlB \tag{14}$$

V is called the Verdet constant, which depends upon both the properties of the medium, the ambient temperature, and the wavelength, λ, of the incident light [11].

- By the Kerr effect, whereby an applied electric field induces birefringence at optical frequencies through the effect of nonlinear optics.
- A non-planar cavity configuration, (i.e., a 4-mirror cavity configuration in which one of the mirrors is out of the plane defined by the other three) introduces a chiral rotation to the polarization of the radiation traveling inside the cavity.

1.3 Optical Rotations

In this section a brief description of the derivation of optical rotation in chiral molecules will be presented. Optical rotation of the incident light through a media could be described as the electro-dipole transitions between the ground state $|\psi_g\rangle$ and an excited state $|\psi_e\rangle$.
The electric and magnetic field for circular polarized light propagating along z-direction are: $\overrightarrow{E_a} = \frac{E_o}{\sqrt{2}}(\hat{x} - ia\hat{y}), \overrightarrow{B_a} = \frac{B_o}{\sqrt{2}}(ia\hat{x} + \hat{y})$, where a=1 for right circular polarized light and left for left polarized light. The transition amplitudes are given by[3] :

$$E_1 = \langle\psi_g|\widetilde{E_1}|\psi_e\rangle \quad (15)$$

$$M_1 = \langle\psi_g|\widetilde{M_1}|\psi_e\rangle \quad (16)$$

Where, $\widetilde{E_1} = \sum_i er_i$ is the electric dipole moment operator and $\widetilde{M_1} = \frac{e\hbar}{2m_e}(\vec{L} + 2\vec{S})$ is the magnetic dipole moment operator. For a pure electric dipole transition or a pure magnetic dipole transition, there is no difference in the absorption probability for right and left circularly polarized light (no circular dichroism).
The symmetry of the E1 and M1 operators is such that E1 transitions can only occur between states of opposite parity (i.e. even ↔ odd), whereas M1 transitions can only occur between states of the same parity (i.e. even ↔ even, or odd ↔ odd). For nonchiral molecules, all states are either even or odd, therefore transitions between states can be either E1 or M1 transitions, but not both[3]. In contrast, in chiral

molecules, the molecular states could be could be of both even and odd character, so that a superposition of E1 and M1 transitions is possible, and the transition amplitude A_a is given by[3]:

$$A_a = \langle \psi_g | \widetilde{E_1} \overrightarrow{E_a} + \widetilde{M_1} \overrightarrow{B_a} | \psi_e \rangle \quad (17)$$

The difference between the transition probability between right circularly polarized light $|A_+|^2$, and left circularly polarized light $|A_-|^2$, normalized by the sum, is given by δ:

$$\delta = \frac{|A_+|^2 - |A_-|^2,}{|A_+|^2 + |A_-|^2} = \frac{n_+ - n_-}{n_+ + n_-} \quad (18)$$

The value of factor δ is a method for identifying the concentration of a particular chiral molecule.

Moreover, the exact value of the dichroism as a function of wavelength δ(λ), from the UV to the IR, gives significant information on the three-dimensional structure of the chiral molecule.

When there is circular birefringence, that is, $(n_+ \neq n_-)$, then linearly polarized light (which is a superposition of right and left circularly polarized light) is rotated by an angle:

$$\varphi = \frac{\pi L}{\lambda}(n_+ - n_-) \quad (19)$$

Where L is the effective pathlength of the light beam inside the optical cavity.

1.3.1 Faraday effect

As mentioned before in chapter 1.2.3, the optical angle of the Faraday effect is given by eq. 14. In this chapter the full derivation will be presented briefly.[4]

Electromagnetic waves propagating through a medium interact with the atoms of that medium by inducing oscillating electric dipoles in the atoms. The force on an electron due to electric and magnetic fields is given by:

$$F_e = e(\vec{E} + \frac{1}{c}\vec{u}x\vec{B}) \quad (20)$$

Assuming that the electromagnetic wave propagates along the direction of the back-ground magnetic field, which we define as the z axis. Then, the electric-field vector and the displacement vector $\vec{s}$ of the dipole

oscillation are restricted to the (x, y) plane. Let us further assume that the oscillation of an individual electron in the atom has a natural frequency ω_o, related to a restoring force constant f = ω_o^2m, where m is the mass of the oscillating electron. Then, the equation of motion of the electron is:

$$\mathrm{m}\frac{d^2\vec{s}}{dt^2} + f\vec{s} = -e(\vec{E} + \frac{1}{c}u\frac{d\vec{s}}{dt}x\vec{B}) \tag{21}$$

The electro-magnetic wave which stimulates the oscillation of the atom, will be in the form of $\vec{E} = \vec{E}_o e^{-i(kz-\omega t)}$.
Thus, the equation. 21 will be:

$$(\omega_o^2 - \omega^2)s_x - i\Omega\omega s_y = \frac{-e}{m}E_x \tag{22}$$

$$(\omega_o^2 - \omega^2)s_y - i\Omega\omega s_x = \frac{-e}{m}E_y \tag{23}$$

where is the cyclotron frequency:Ω=$\frac{Be}{mc}$, also we define $E_{\pm} \equiv E_{\mathrm{x}} + iE_y$ and $s_{\pm} \equiv s_{\mathrm{x}} + is_y$. Therefore, the equations (22), (23) will be:

$$(\omega_o^2 - \omega^2 - \omega\Omega)s_+ = \frac{-e}{m}E_+ \tag{24}$$

$$(\omega_o^2 - \omega^2 - \omega\Omega)s_- = \frac{-e}{m}E_- \tag{25}$$

By solving the previous 2x2 system and also combing the formula $P_{\mathrm{s,x}} = n_e e s_{x,y}$, we have:

$$P_{\pm} = \frac{n_e e^2 E_{\pm}}{m(\omega_o^2 - \omega^2 \mp \omega\Omega)} \tag{26}$$

where ne is the number density of electrons, we can find the polarizability $\chi_{\pm} \equiv 4\pi\,\frac{\mathrm{P}\pm}{\mathrm{E}\pm}$ and then $e_r \equiv 1 + \chi_{\pm}$ which is called electric permeability, hence, the index of refraction for left-handed and right handed circularly polarized waves as:

$$n_{\pm} = \sqrt{\frac{n_e e^2 4\pi}{m(\omega_o^2 - \omega^2 \mp \omega\Omega)} + 1} \tag{27}$$

Obviously, left and right polarized components with of the linearly polarized light will travel a with different velocities in the medium, which induce a relative angle to the angle of the polarization given by

$$\Phi = \frac{\omega}{2c}(n_+ - n_-)z \tag{28}$$

By making the approximation:

$$(n_+ - n_-) \approx \frac{n_e e^2 \omega 4\pi\Omega}{m(\omega_o^2 - \omega^2)^2} \tag{29}$$

so that the change of the polarization angle with propagation distance is given by:

$$\mathrm{d}\varphi = \int_0^l \frac{n_e e^2 \omega 4\pi\Omega}{cm(\omega_o^2 - \omega^2)^2} dz \tag{30}$$

Equation (30) is nothing different but equation (14).

A qualitatively way to visualize Faraday effect is the following:

In general, near an atomic transition, a photon is absorbed when $h/c\lambda = E_f - E_i$ is satisfied, where E_f and E_i are the final and initial state energies, respectively. An introduction of an external magnetic field, as in the case of the Faraday effect, the energies of the initial and final states may have degeneracies removed, depending upon the angular momentum of each state, resulting in an energy shift for the states, which is the known Zeeman effect. As a result, each state has a different magnetic moment that couples to the external field via $-\mu s B$, where μs is the magnetic moment of state 's'. For visualization, consider a system where each atom contains a nondegenerate ground state, with a Zeeman triplet forming excited state, with nuclear spin 0 and no hyperfine structure. This corresponds to a $S_0^1 - P_1^1$ transition of an atom, where in an external field, the upper-state level splits with an energy shift $\Delta \mathrm{E} = \pm \mu_\mathrm{B} \mathrm{B}$ for the m=±1 states, where μ_B is the Bohr magneton.

Furthermore, when light is incident upon and interacts with the medium, angular momentum must be conserved, and the electric dipole selection rules dictate that only the resonant transitions to higher energy occurs for Δm=±1. Right circularly polarized light carries angular momentum of -1, and left circularly polarized light has angular momentum of +1. This results in each circular polarization component interacting with its own two-level system, indicating that each polarization will propagate through the medium with different speeds, and hence different indices of refraction; thus, medium becomes birefringent[5].

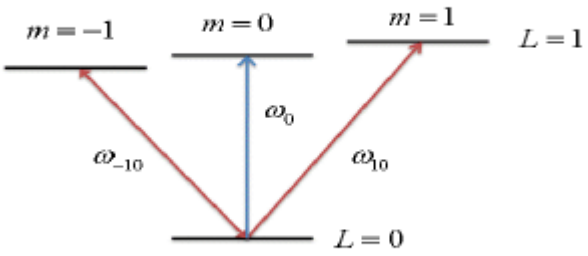

Figure 10-The ground state has n=0 and L=0, while the first excited state has n=1 and L=1. A longitudinal magnetic field splits the magnetic field sublevels.

1.3.2 Non-Planarity

A nonplanar cavity configuration, in which one of the mirrors is out of the plane defined by the remaining mirrors, induces a chiral rotation to the polarization of the radiation traveling inside the cavity. In this section will be presented a brief explanation how non planarity induces optical rotation, NPI-OR[6].

Theory: The NPI-OR can be calculated as follows: Assuming we have a four-mirror bow-tie cavity and the light path of the pulse will be as it is shown in figure 11. Defining $\vec{k}_{12}$,$\vec{k}_{23}$,$\vec{k}_{34}$,$\vec{k}_{41}$ the unit propagation vectorsalong each leg. Assuming M1 is the origin of the light path. The next step is to calculate these vectors as a function of the cavity's parameters (length l and width w). Then for each reflection, the incident and the reflected wave vectors in the principal axis system of the reflector are calculated. The cross product of successive propagation vectors gives the perpendicular component (in the plane of

incidence) for each reflector, i.e., $\vec{k}_{ij}\times\vec{k}_{jk} = \vec{s}_{Mj}$, while, thecross product of$\vec{s}_{Mj}\times\vec{k}_{ij}$, gives the parallel component (in theplane of incidence), i.e.,

$\vec{s}_{Mj}\times\vec{k}_{ij} = \vec{p}_{Mj}$.Thus, the state of polarization after each reflection could be calculated. After all reflections, the resulting final polarization has an angle with the initial and under the assumptions of l > w ≫ h, we obtain a closed analytical expression for the NPI-OR angle:

$$\sin a_c = 2\frac{\left(-l + \sqrt{l^2 + w^2}\right)\gamma}{w} \tag{31}$$

Where $\gamma = \tan^{-1}(h/l)$, h is the off-plane height of M4, w is the distance between M2 and M4 (M1 and M3), and l is the distance between M1 and M4 (M2 and M3). For w ≪ l, we get:

$$\sin a_c = \frac{hw}{l^2} \tag{32}$$

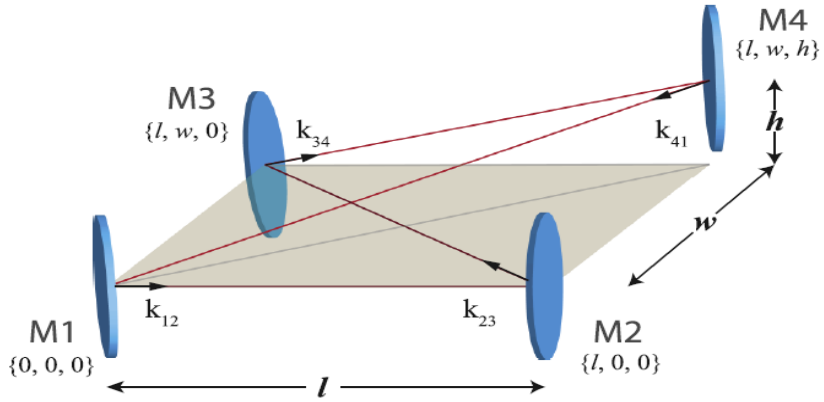

Figure 11 Non planar chiral rotation is induced by placing the M4 mirror out of the plane which is defined by the three other mirrors. [6]

1.4 Cavity Ring down Polarimetry

The basic setup of the single-pass polarimeter has barely changed in the two centuries since its first demonstration by Biot in 1815 [7]. As It is shown in Figure12, two polarizers are crossed at 90°, so that no light is transmitted. Subsequently, an optically active sample is added which rotates the linear polarization between the two polarizers by an angle ϕ, so that now some light is transmitted. Finally, the second polarizer (the analyzer) is rotated by the angle needed to null the transmission again, thus determining experimentally the angle ϕ (Fig. 12.B). However, the sensitivity of the determination of ϕ is limited by the mechanical properties of the rotation stage of the analyzer; practically this limits the sensitivity of this method to 0.01–0.1°.

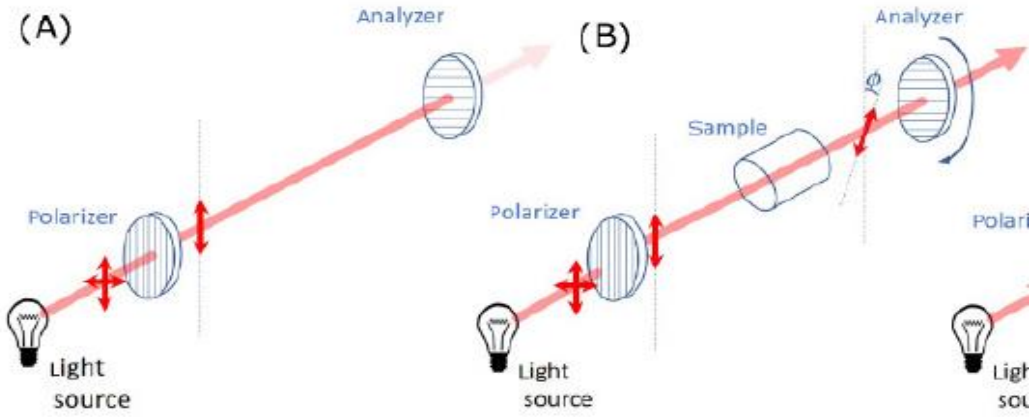

Figure 12(A) Extinction polarimeter, with crossed polarizers, (B) analyzer rotated by angle φ to find extinction caused by rotation by sample of angle φ.[3]

The improvement of the sensitivity in spectroscopy is succeeded by passing the light beam through the sample many times has been offered by using an optical cavity. Optical cavities offer a method for ultrasensitive absorption measurements with very long pathlengths, of typically a few kilometers, and up to approximately 100 km (e.g. a cavity of length 1 m, with mirrors of reflectivity R = 99.999% can produce an average of 10^5 cavity passes, for a total pathlength of 100 km and subsequently the active length of the chiral medium increases by a factor of 10^5).

The simplest setup that can be used as a cavity typical consists of 2 curved mirrors facing each other and aligned so that the light entering reflects back and forth in the cavity.

The absorption is detected by measurement in the decrease in the photon lifetime of a short laser pulse lifetime τ in the cavity (compared to an empty cavity, with $\tau = \tau_o$), which appears as an exponential decay, or "ring down":

$$I = I_o e^{-t/\tau} \qquad (33)$$

However, only with this setup it is impossible to measure the chiral rotation because this angle will be canceled out by the returning beam from the second mirror.

The solution to this problem is to insert two (low-loss)quarter-wave plates (which are antireflection coated) in that cavity[8], on either side of the sample, with their optical axis at an angle ($90° - \alpha$) to each other (where α is a small angle, typically, $\alpha \approx 3°$).Circularly polarized light is inserted into the cavity and it then becomes linearly polarized between the intracavity quarter-waveplates. The linearly polarized light is then rotated by angle 2α

per cavity round trip, for the empty cavity. When a chiral substance is inserted in the cavity, the chiral rotation is ϕc per cavity pass and 2α per cavity round trip, which gives a total rotation of 2(α+ ϕc) per cavity round trip. When the cavity output is passed through a polarizer before the detector, the experimental signals are modified compared to Eq. (33). In addition to the exponential decay, there is also an oscillating term, from the polarization rotation (similar polarization beatings from intracavity linear birefringence were first seen by Jacob et al.[9]):

$$I = I_o e^{-t/\tau} \cos^2(\omega t + \varphi) \tag{34}$$

where ω is the polarization rotation frequency, given for an empty cavity by

$$\omega = \omega_o = \frac{2\alpha}{t_{roundtrip}} = \frac{2ac}{d} \tag{35}$$

Where,$t_{roundtrip} = 2\mathrm{d}/\mathrm{c}$ is the cavity roundtrip time, and d is the mirror separationdistance. For a cavity with a chiral sample, ω is given by

$$\omega = \omega_c = \frac{2(\alpha + \varphi_c)}{t_{roundtrip}} = \frac{(\alpha + \varphi_c)c}{d} \tag{36}$$

Therefore, if frequencies ω_o (for an empty cavity) and ω_c (for a cavity with chiral sample) are measured, then the single-pass chiral optical rotation angle is given by:

$$\varphi_c = \frac{(\omega_c - \omega_o)\mathrm{c}}{d} \tag{37}$$

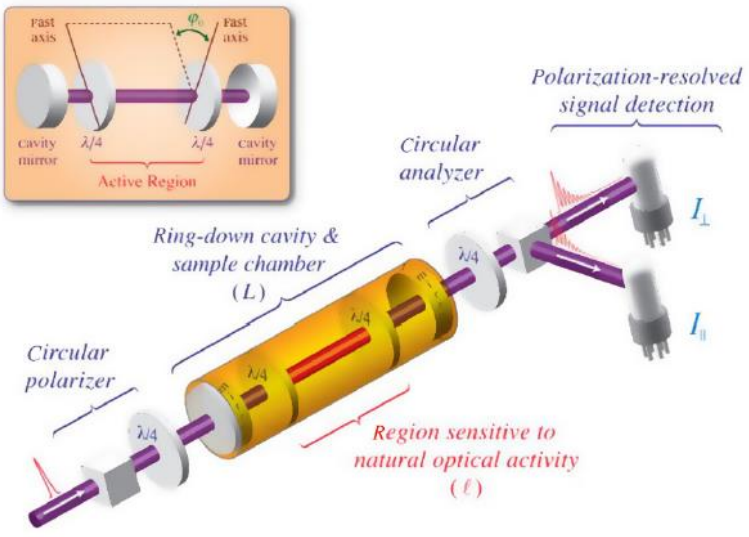

Figure 13Experimental setup for two-mirror CRDP. Abbreviation: CRDP, cavity ringdownpolarimetry[3].

An essential limiting factor, for both single-pass and cavity-enhanced cases, is the ability to measure the null sample, needed as a reference for the signal of the chiral sample. The removal of the sample often introduces errors to the measurement system, as there will be small changes to the alignment, positioning, background birefringence, etc. The solution to deal with this problem is to use a ring cavity with to beams with opposite direction (which we label as clockwise CW, and counterclockwise CCW),) as it is shown in figure 14. In addition, it is possible to take advantage of Faraday effect to further cancel out any spurious birefringence and offsets in the experiment. When magnetic field in applied to a transparent crystal, the Faraday effect causes a rotation of the plane of polarization which is linearly proportional to the component of the magnetic field in the direction of propagation
There are transparent crystals with a large Faraday effect known as magneto-optic crystals, which have a large Verdet constant, such as TGG. TGG absorbs less than10^{-4} cm $-$ 1 from about 500–1400 nm, can be antireflection coated so that it is compatible with a low-loss cavity, and has a Verdet constant of 192 rad T $-$ 1 m $-$ 1 at 532 nm.

The sign of the Faraday rotation angleθ_F is determined by the magnetic field direction B and not by the direction of propagation of the light (as is the case for chiral optical rotation). This difference in symmetry, between Faraday rotation θf and chiral rotation ϕ_c, leads to a very interesting result when both are present in a ring cavity: the total single-pass rotation angle for CW and CCW, Θ_{CW} and Θ_{CCW}, are different (breaking the symmetry between CW and CCW), as in one case the two angles add, and in the other case the two angles subtract:

$$\Theta_{cw} = \theta_F + \varphi_c, \omega_{cw} = \theta_F + \varphi_c \frac{c}{L} \quad (38)$$

$$\Theta_{ccw} = \theta_F - \varphi_c, \omega_{ccw} = \theta_F - \varphi_c \frac{c}{L} \quad (39)$$

The sign of the Faraday rotation angle $\theta_F$is depended by the sign of the applied magnetic field B, so that the polarization beating frequencies can be written as:

$$\omega_{cw}(\pm \mathrm{B}) = (\pm\theta_F + \varphi_c)\frac{c}{L} + \omega_{offset}(t) \quad (40)$$

$$\omega_{ccw}(\pm \mathrm{B}) = (\pm\theta_F - \varphi_c)\frac{c}{L} + \omega_{offset}(t) \quad (41)$$

Where,$\omega_{offset}(t)$ include all nonideal, time-dependent offset and noise terms, such as from poor cavity alignment and from residual birefringence.

Therefore, the difference in the polarization beating frequencies Δω(±B) is given by:

$$\Delta\omega(\pm B) = |\omega_{cw}(\pm B)| - |\omega_{ccw}(\pm B)| = \pm 2\varphi_c \frac{c}{L} \quad (42)$$

Furthermore, the additional subtraction of the two frequencies with opposite magnetic field gives:

$$\Delta\omega(+B) - \Delta\omega(-B) = 4\varphi_c \frac{c}{L} \quad (43)$$

These signal reversals allow the determination ofϕc without needing to remove the chiral sample, but simply by comparing the polarization beating frequencies of CW and CCW (i.e. one direction provides a background reference for the other), and an additional check is given by reversing the applied magnetic field. Notice, that the $\omega_{offset}(t)$ is also canceled out.

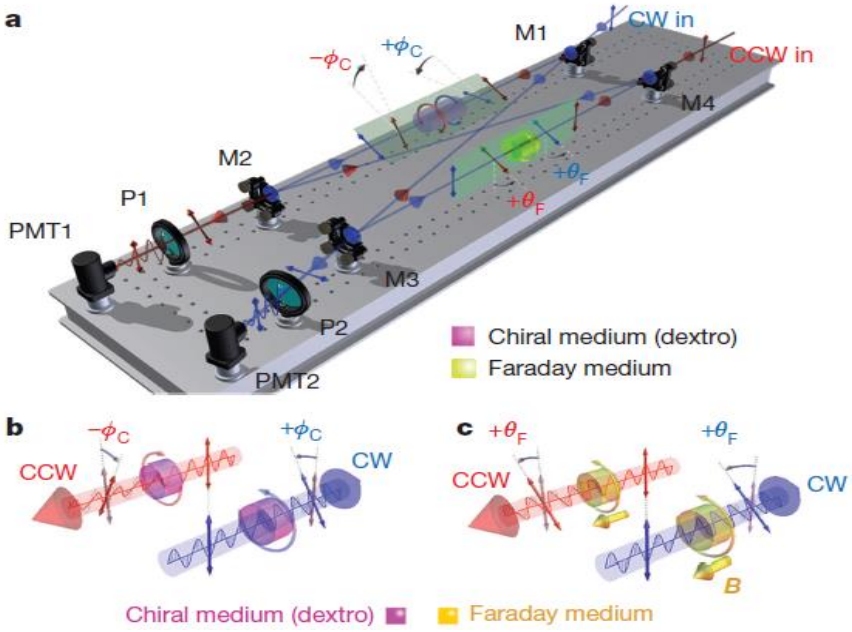

Figure 14: The layout of four mirrors (M1–M4), polarizers (P1, P2), photomultiplier tubes (PMT1,PMT2), the chiral sample, the Faraday medium and the counter-propagating laser beams (CW and CCW). b, The chiral sample gives opposite laboratory frame optical rotations for CW and CCW[10]

1.5 Experimental setup and analysis

In this section will extensively be described the procedure of the measurement of optical rotation produced by chiral liquid solutions. The experimental set up which is used is illustrated in figure 15.

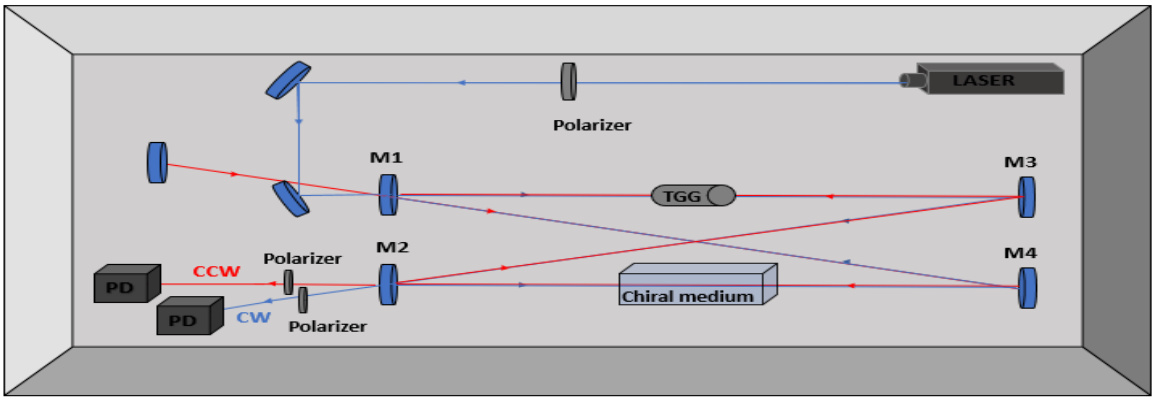

Figure 15 Experimental setup

The 532 nm output of a 10 µJ, 8 ns FWHM Nd:YAG DPSS laser (Roithner RLTMPL-532-100), operating at a repetition rate of 10 kHz, is split in two equal parts and is injected in a bowtie optical cavity. A polarizer is employed before the cavity to ensure that only polarized light insert the cavity with s-polarization. The cavity comprises two high reflectivity mirrors (Layertec, R > 99.98%) and two high reflectivity, low loss output couplers (Layertec, R > 99.5%). The total free-space cavity length is 4.8m. In our setup, the TGG induces a rotation of the linear polarization plane of ~25 degrees per pass. A 3 mm thick flow cell is used to introduce the liquid solution (Fructose, Maltodextrin, Lysozyme), composed of 2 AR-coated windows, with one side AR- coated for an air-fused silica interface, and the other side AR-coated for a water-fused silica interface. The main limiting factor of the photon lifetime is the flow cell, specifically from losses from the interior interfaces between the sample and the window. Since the absorption of the sample at 532 nm should be negligible, losses arise from coating imperfections or degradation at the window-sample interface, which produce scattering. Two thin-film polarizers are employed after the cavity, to measure the projection of the rotating polarization plane. The signal is detected by two Biased Si Photodiodes (Thorlabs DET36A), and recorded by an oscilloscope with a sampling rate up to 10 Gs/s, and a maximum bandwidth of 3 GHz. The oscilloscope monitors four signals; the two photodiode outputs; the laser trigger; and the magnetic field signal. The coil used to produce the magnetic field applied to the TGG crystal is driven using custom electronics and its direction can be inverted at a repetition rate that can be varied between 0.1 and 100 Hz. A home-made software monitors the status signal of the

magnetic field reversal circuit. When change in the status signal is detected (i.e., the magnetic field is reversed), the average of a predetermined number of pulses is recorded. For each consecutive round trip of the pulse through the cell, the polarization plane is rotated by a finite angle. Therefore, by placing polarizers in the output of the two modes, we observe a time-dependent signal which has the form a damped oscillation:

$$y(t) = e^{-t/\tau} cos^2(\omega t + \varphi) \qquad (44)$$

where τ the decay time, ω the angular frequency, and ϕ is the initial phase of the oscillation. The frequency ωid deduced by following the procedure which is described in section 1.4 (equations 42,43). Thus, the most of the noise is consider to be canceled out. More precisely, the benefit of the signal reversals is the cancellation of drifts, which can arise from temperature variations or mechanical in- stabilities which affect the beating frequency. An example of this is demonstrated in figure-----

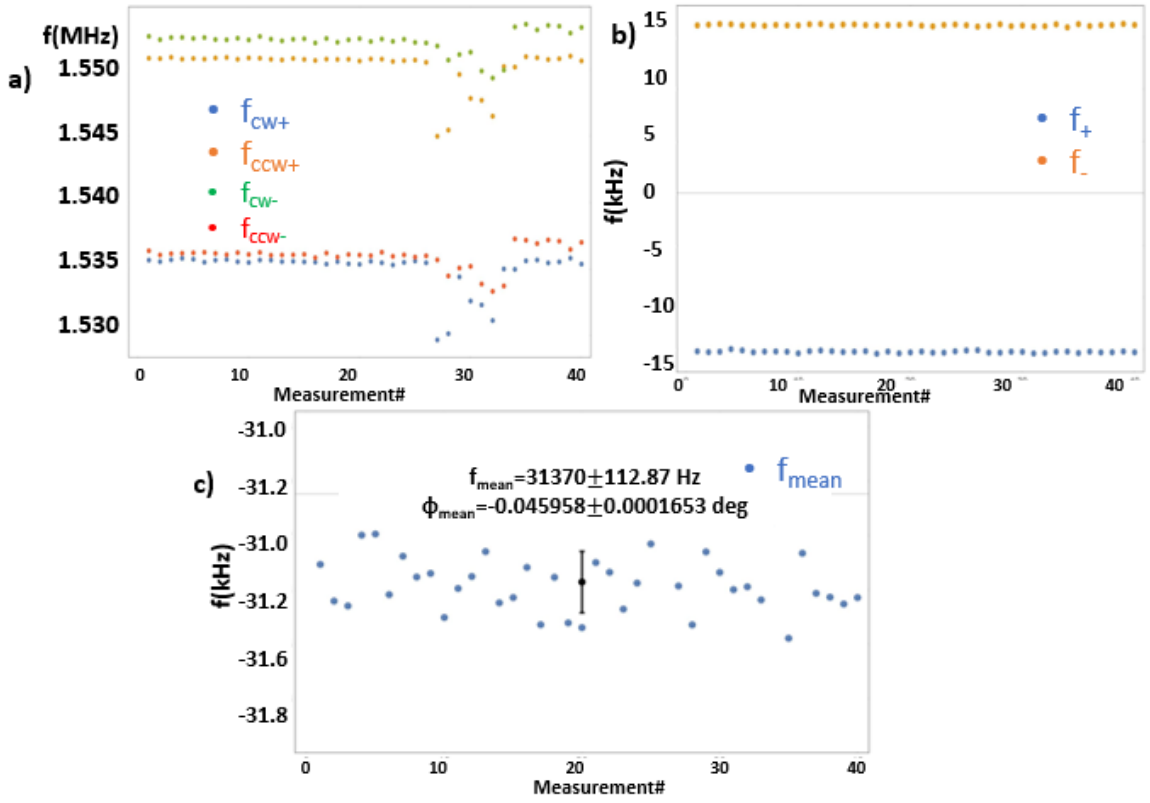

Figure 16: a)Consecutive measurements off$_{cw+}$,f_{ccw+} ,f_{cw+} ,$f_{ccw-}$with unexpected noise. b) $f_{\pm} = |f_{cw\pm}| - |f_{ccw\pm}|$cancel out the most of this unexpected noise, c) $f_{mean} = \frac{f_+ - f_-}{measurements\#}$, second abstraction for further clearing the frequency beating to better define the optical rotation angle

However, equation 44 does not fully describe our signal, since some spurious linear birefringence may reduce the modulation depth. In addition, low pass filter from oscilloscope or the photodiodes induce a non-zero offset. In order to take into account these effects the form of the damped oscillation is modified to:

$$y(t) = (e^{-\frac{t}{\tau}} + Be^{-\frac{t}{\tau_2}})\, cos^2(\omega t + \varphi) + c \tag{45}$$

where now b and τ_2 are the amplitude coefficient and the decay time of the exponential introduced to account for the reduced modulation depth and c is the voltage offset.

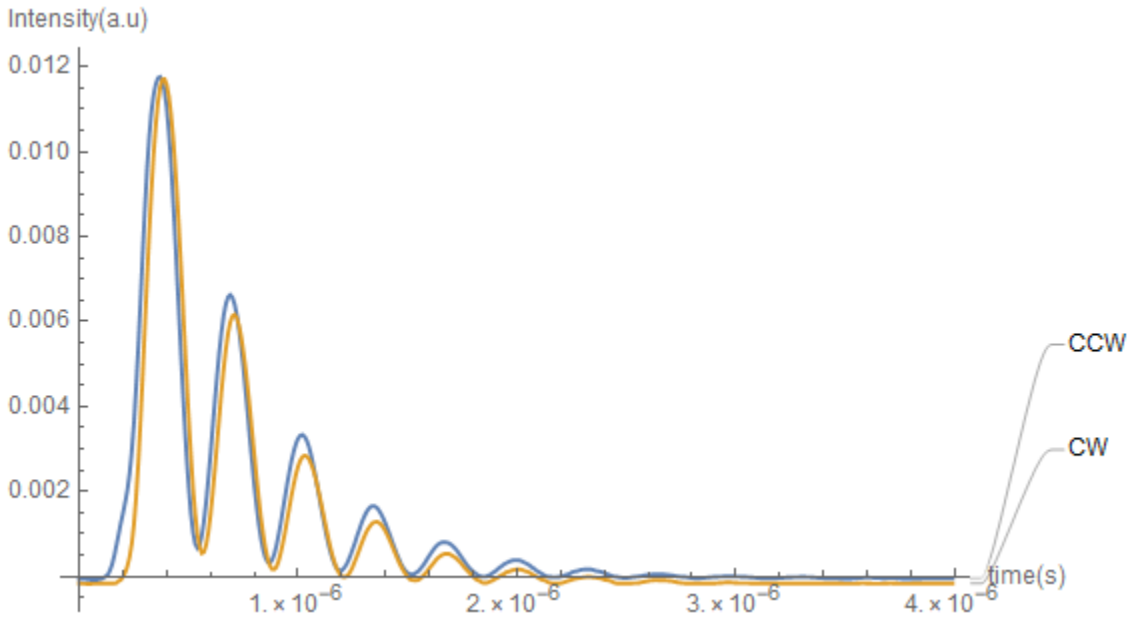

Figure 17: Experimental signals showing the polarization oscillation frequencies CW and CCW in the exponential decay

The value of the angular frequency can be extracted by regression analysis, where the signal is fitted with a suitable model, similar to equation 45.

The main limitation factor to our data acquisition scheme is the inability to capture of light pulses emitted from the Laser. Typically, oscilloscopes have rise time about some millisecond, which in our instrument results exhibits a loss of roughly 99% of the emitted pulses, since the laser repetition rate is 10 kHz. A possible remedy to this, is that instead of using oscilloscope in the detection scheme, to employ a dedicated data acquisition card described in [11].In this way, the measurement duration will be reduced by a factor of

100 and also, much faster signal reversals at 10–100 Hz instead of 0.1 Hz, will likely improve the sensitivity further, by canceling slow drifts.

1.5.1 Chirality measurements in liquid solutions

The solutions that are measured are water-Fructose (0.0125-0.6% gr/ml) and water-Maltodextrin (0.00625-0.3% gr/ml).

Maltodextrin

The maltodextrin was introduced in the AR coated flow cell and the optical rotation is measured for each concentration as it is shown in figure 16

The optical activity of Maltodextrin is found $[a]_{532} = +371.503 \pm 1.51704$

Fructose

The maltodextrin was introduced in the AR coated flow cell and the optical rotation is measured for each concentration.

The optical activity of Fructose is found $[a]_{532} = -176.824 \pm 1.1229 \frac{\text{deg ml}}{dm\ g}$.

Finally, a graph summing up all the data from both Fructose and maltodextrin is depicted below.

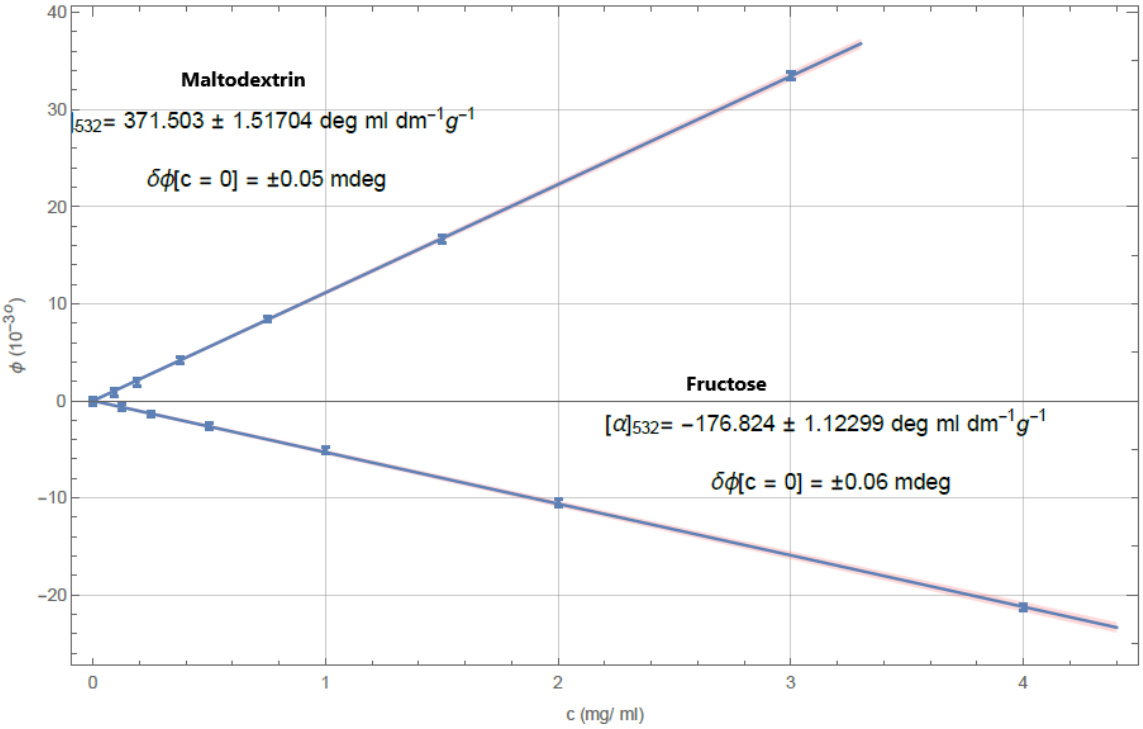

Figure 18: Optical rotation of Maltodextrin and Fructose as a function of concentration of the solutions.

1.5.2 Chirality measurements in Biological samples

Lysozyme is an enzyme found in secretions of animals and humans, such as tears, sweat and saliva. It is part of the innate immune system, having antibacterial effects; for example, it eliminates bacteria found in tears, and therefore its abundance in tears is a sign of a healthy eye. The normal level of Lysozyme in tears has been measured to be 1.5 mg/ml. But, in patients with dry eyes has been measured to be about 0.5-0.7 mg/ml. In this experiment, due to the difficulty in finding an adequate amount of tears from different patients, solution with similar concentrations are produced.

The samples of various Lysozyme concentrations were obtained by diluting a 10 mg/ml aqueous (ph = 7) solution of Lysozyme from chicken egg white (Sigma Aldrich, 98% protein), previously stored at 20 °C. The results of the measurements are illustrated in figure 19

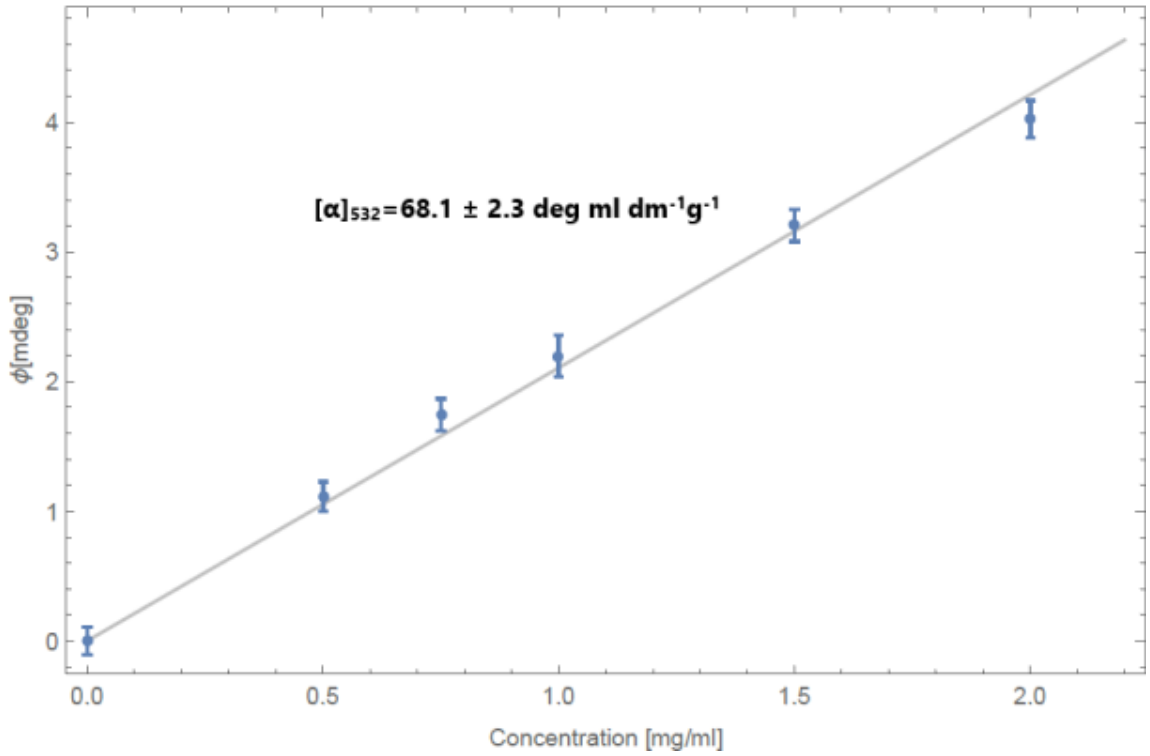

Figure 19: Optical rotation measurements of lysozyme solution in concentrations ranging from 0 to 2 mg/ml

The extracted value for the specific rotation at 532 nm reported here is 68.1 ± 2.3 $\frac{\text{deg ml}}{dmg}$, and it is in good agreement with the expected value at 532 nm.In bibliography the optical activity of lysozyme is reported for at 589nm[12] , 365 nm[13] and at 578 nm[14]. In addition, in reference [11] is reported in the dependence of optical activity as a function of wavelength, with two different models: the Moffitt-Young and the Shechter-Blout. The discrepancy between the models and our measurement is attributed to reason that the optical activity varies significantly with pH or depending on the molecule's origin, for example if the molecule is of human origin or of white-egg origin[15].

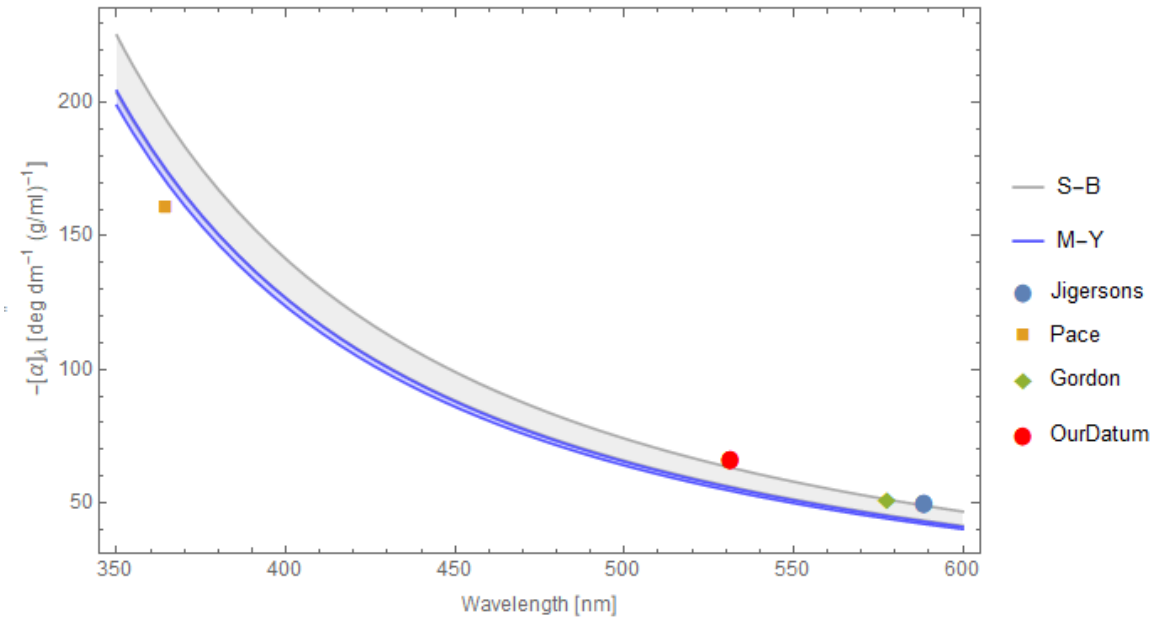

Figure 20: Specific Optical Rotation of lysozyme as a function of wavelength

1.5.3 Chirality measurements in gasses

Part 2: Magnetometry with Spin Polarized Atoms

In this chapter, the fine structure corrections to the non-relativistic Schrödinger equation will be presented and we will focus on spin-orbit interaction term, which is distinguished to the LS and JJ Coupling Scheme. Furthermore, the mathematical tool for the operation of angular momentum eigenvectors will be displayed (special rotations and Glebsch-Gordan coefficients). In addition, the Hyperfine structure that describes the interaction between the magnetic field induced by the electron motion with the nuclear magnetic moment will by studied. Then, we will introduce a new method to produce and spin-polarized atoms through photodissociation in extremely high densities. Based on this fact, we will also suggest a new method to detect magnetic fields with high sensitivity within a few nanoseconds. Finally, the theoretical description of the model as well as the experimental confirmation will be presented.

2.1 Fine Structure

The fine structure describes the splitting of the spectral lines of atoms due to electron spin and relativistic corrections to the non-

relativistic Schrödinger equation. It was first measured precisely for the hydrogen atom by Albert A. Michelson and Edward W. Morley in 1887[16], laying the basis for the theoretical treatment by Arnold Sommerfeld, who intoduced the fine-structure constant. The fine structure energy corrections can be obtained by using perturbation theory. To perform this calculation one must add the three corrective terms to the Hamiltonian: the leading order relativistic correction to the kinetic energy, the correction due to the spin-orbit coupling, and the Darwin term coming from the quantum fluctuating motion or zitterbewegung of the electron.

These corrections can also be obtained from the non-relativistic limit of the Dirac equation, since Dirac's theory naturally incorporates relativity and spin interactions.

$$H = mc^2 + \frac{p^2}{2m} - \frac{e^2}{r} + H_{FS} \tag{46}$$

Where H_{FS} is given by:

$$H_{FS} = -\frac{p^4}{8m^3c^2} + \frac{\hbar^2 p^2}{2m^2c^2r^3}\vec{L}\vec{S} - \frac{\hbar^2 p^2}{8m^2c^2}\nabla^2\frac{e^2}{r} \tag{47}$$

The relativistic contributions can be described as the kinetic, spin-orbit, and Darwin terms, H_{kin}, H_{so}, and H_{Dar}, respectively. Each has a straightforward physical interpretation.

Kinetic contribution

We take the relativistic approximation into account: the total electron energy is E $= \sqrt{(m^2c^2)^2 + (pc)^2}$. The kinetic energy is$T = E - mc^2 = mc^2\sqrt{1 + \frac{p^2}{m^2c^2}} - 1 = \frac{p^2}{2m} - \frac{p^4}{8m^3c^2} + \cdots$

Thus, H_{kin}=$-\frac{p^4}{8m^3c^2}$[17]

Spin Orbit-Interaction

According to Dirac theory the electron has an intrinsic angular momentum ħs and a magnetic moment $\vec{\mu}_e$=$g_e\mu_B\overrightarrow{S}$, where g_e=2 and μ_B=e$\frac{e\hbar}{2mc}$[18]. As the

electron moves through the electric field of the proton it “sees” a magnetic field:

$$B_{mot} = \frac{\vec{U}\mathrm{x}\vec{E}}{c} = \frac{\vec{U}}{c}\frac{\mathrm{x\ e}\vec{r}}{r^3} = \frac{\mathrm{e}\hbar\vec{L}}{mcr^3} \tag{48}$$

However, there is another contribution to the effective magnetic field arising from the Thomas precession. The relativistic transformation of a vector between two moving co- ordinate systems, which are moving with different velocities, involve not only a dilation, but also a rotation[17] .The rate of rotation, the Thomas precession, is:

$$\vec{\Omega}_T = \frac{\vec{a}\mathrm{x}\vec{u}}{2c^2} \tag{49}$$

However, for a vector fixed in a co-ordinate system moving around a circle, as in the case of the spin vector of the electron as it circles the proton, Thomas precession occurs. From the point of view of an observer fixed to the nucleus, the precession of the electron is identical to the effect of a magnetic field

$$\vec{B}_T = \frac{1}{\gamma_e}\vec{\Omega}_T \tag{50}$$

Substituting $\gamma_e = \frac{e}{mc}, a = \frac{e^2\hat{r}}{mr^3}$ into equation (48) gives,

$$\vec{B}_T = -\frac{1}{2}\frac{\mathrm{e}\hbar\vec{L}}{mcr^3} \tag{51}$$

This gives rise to a total spin-orbit interaction

$$H_{SO} = \frac{e^2\hbar^2}{2m^2c^2r^3}\vec{L}\vec{S} \tag{52}$$

The Darwin Term

Electrons exhibit "Zitterbewegung", fluctuations in position on the order of the Compton wavelength, $\hbar$/mc. As a result, the effective Coulombic potential is not V(r), but some suitable average $\bar{V}$(r), where the average is

over the characteristic distance $\hbar$/mc. To evaluate this, we expand V(r) about r in terms of a displacements,

$$V(r+s) = V(r) + \vec{\nabla}Vs + \frac{1}{2}\sum_{ij} s_{xi}s_{yj}\frac{\partial^2 V}{\partial_{x_i}\partial_{y_j}} + \tag{53}$$

Assume that the fluctuations are isotropic. Then the time average of $V(r+s) - V(r)$is:

$$\Delta \mathrm{V} \sim \frac{1}{2}[\frac{1}{3}\left(\frac{\hbar}{mc}\right)^2]\nabla^2 V = -\frac{1}{6}\frac{e^2\hbar^2}{m^2c^2}\nabla^2(\frac{1}{r}) \tag{54}$$

The precise expression for the Darwin term is[17]:

$$H_{DAR} = -\frac{1}{8}\frac{e^2\hbar^2}{m^2c^2}\nabla^2\left(\frac{1}{r}\right) \tag{55}$$

The coefficient of the Darwin term is 1/8, rather than 1/6. Recall that $\nabla^2\left(\frac{1}{r}\right) = 4\pi\delta(r^3)$, so that the Darwin term is nonzero only for SS states, where $\langle S|H_{Dar}|S\rangle$>0. That is, the Zitterbewegung effectively cuts off the cusp of the 1/r potential, thereby reducing the binding energy for S-electrons.

2.1.1 Clebsch-Gordan Coefficients

In classical mechanics, the total angular momentum J of a system composed of two parts, one with angular momenta j_1 and the other with j_2, is given by the vector addition of j, and j_2 :

$$J = j_1 + j_2 \tag{56}$$

There are two useful points of view in describing such a compound system. One complete set of commuting angular momentum operators is j_1^2,j_2^2,j_{1z},j_{2z}.The states $|j_1m_1\rangle|j_2m_2\rangle \equiv |j_1m_1, j_2m_2\rangle$ are simultaneous eigenfunctions of these operators:

$$j_1^2|j_1m_1, j_2m_2\rangle = j_1(j_1+1)\,|j_1m_1, j_2m_2\rangle$$
$$j_{1z}|j_1m_1, j_2m_2\rangle = m_1|j_1m_1, j_2m_2\rangle$$
$$j_2^2|j_1m_1, j_2m_2\rangle = j_2(j_2+1)\,|j_1m_1, j_2m_2\rangle$$

$$j_{2z}|j_1 m_1, j_2 m_2\rangle = m_2|j_1 m_1, j_2 m_2\rangle \tag{57}$$

Here the $|j_1 m_1, j_2 m_2\rangle$ states are called the uncoupled representation and span a space of dimension $(2j_1 + 1)(2j_2 + 1)$.

It is easily verified that another complete set of commuting angular momentum operators is $j_1^2, j_1^2, J^2 = j_1^2 + j_2^2$ and $J_z = j_{1z} + j_{2z}$. The states $|\mathrm{JM}\rangle$, which are simultaneously eigenfunctions of these operators, are called the coupled representation and span a space of dimension 2 j + 1 for each j value. It is also common to write $|j_1 j_2\, JM\rangle$ for $|\mathrm{JM}\rangle$, but we prefer to use in general the more compact notation. These notations correspond to equation [58].

$$\begin{gathered} j_1^2|\mathrm{JM}\rangle = j_1(j_1 + 1)\ |\mathrm{JM}\rangle \\ J^2|\mathrm{JM}\rangle = J(J + 1)|\mathrm{JM}\rangle \\ j_2^2|\mathrm{JM}\rangle = j_2(j_2 + 1)\ |\mathrm{JM}\rangle \\ j_z|\mathrm{JM}\rangle = \mathrm{m}\ |\mathrm{JM}\rangle \end{gathered} \tag{58}$$

Hence these two descriptions are equivalent and the two representations are connected by:

$$|JM\rangle = \sum_{m_1 m_2} C(j_1 j_2; m_1 m_2)|j_1 m_1, j_2 m_2\rangle$$

or

$$|j_1 m_1\rangle|j_2 m_2\rangle = \sum_{J,M} C(j_1 j_2; m_1 m_2)\ |JM\rangle \tag{59}$$

where the elements of the unitary transformation, called Clebsch-Gordan coefficients, are chosen to be real. We make the formal identification

$$C(j_1 j_2; m_1 m_2) \equiv \langle j_1 m_1 j_2 m_2|JM\rangle \tag{60}$$

The orthonormality of $|JM\rangle$ and $|j_1 m_1, j_2 m_2\rangle$ leads to the orthogonality relations:

$$\sum_{m_1 m_2} \langle JM|j_1 m_1, j_2 m_2\rangle\langle j_1 m_1, j_2 m_2|J'M'\rangle = \delta_{JJ'}\delta_{MM'} \tag{61}$$

and

$$\sum_{m_1 m_2} \langle JM|j_1 m_1, j_2 m_2\rangle\langle j_1 m_1', j_2 m_2'|JM\rangle = \delta_{m_1 m_1'}\delta_{m_2 m_2'} \tag{62}$$

2.1.2 Rotation Matrices

In this section the general transformation problem of angular momentum under rotation will be described. For an arbitrary rotation about $\hat{n}$ by an angle a, we obtain:

$$R_n(a) = e^{-ia\vec{J}\hat{n}}, where\ \vec{J}\hat{n} = -\frac{i\partial}{\partial a} \quad (63)$$

any finite rotation may be uniquely specified by giving the three components of the vector a$\hat{n}$, where a is the angle of rotation and $\hat{n}$ is a unitvector pointing along the axis of rotation. For many purposes, however, an equivalentbut more useful description is achieved by introducing the three Euler angles ϕ, and χ as shown in figure. The Euler angles ϕ, θ, and χ should be regarded as defining a prescription whereby the F = XYZ frame may be made to coincide with the g = xyz frame (the body-fixed frame) by three successive finite rotations.

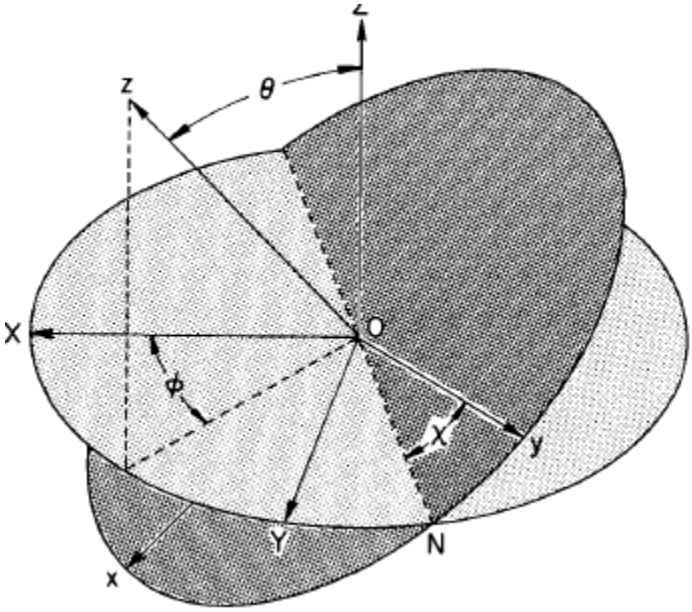

Figure 21 Euler angles φ,θ, and χ relating the space-fixed F = XYZ and molecule-fixedg = xyz frames.[19]

1. A counterclockwise rotation ϕ about 2, the vertical axis. This carries the Y axis into the line of nodes N
2. A counterclockwise rotation θ about the line of nodes N. This carries the Z axis into the z axis (the figure axis of the body).
3. A counterclockwise rotation x about z, the figure axis. This carries the line of nodes N into the y axis.

Thus, the equation [63] is transformed to

$$R(\varphi,\theta,\chi) = e^{-i\chi\vec{J}\hat{n}_x}e^{-i\theta\vec{J}\hat{n}_\theta}e^{-i\varphi\vec{J}\hat{n}_\varphi} = \quad (64)$$

$$e^{-i\chi\vec{J}_z}e^{-i\theta\vec{J}_N}e^{-i\varphi\vec{J}_z}$$

After a trivial process that is explicitly described in [19] the rotation matrix above could be expressed as :

$$R(\varphi,\theta,\chi)|JM\rangle = \sum_{M'} D^J_{M,M'}(\varphi,\theta,\chi)|JM'\rangle \tag{65}$$

Where, the expression coefficients

$$\langle JM|D^J_{M,M'}(\varphi,\theta,\chi)|JM'\rangle \tag{66}$$

Where,

$$D^J_{M,M'}(\varphi,\theta,\chi) = e^{-i\varphi M'}d^J_{M,M'}(\theta)e^{-i\chi M} \tag{67}$$

As Wigner first demonstrated, the $d^J_{M,M'}(\theta)$ can be expressed as a finite polynomial in arguments of the θ/2:

$$d^J_{M,M'}(\theta) = [(J+M)!\,(J-M)!\,(J+M')!\,(J-M')!]^{\frac{1}{2}} \tag{68}$$
$$\text{x}\sum_v \frac{(-1)^v}{(J-M'-v)!(J+M-v)!(v+M'-M)!v!}$$
$$\text{x}\left[\cos\frac{\theta}{2}\right]^{2J+M-M'-2v}\left[\sin\frac{\theta}{2}\right]^{M'-M+2v}$$

where the sum over v is for all integers for which the factorial arguments are nonnegative.

The $d^J_{M,M'}(\theta)$ satisfy a number of useful symmetry relations:

Substituting M→ −M', and M'→ −M:

$$d^J_{M,M'}(\theta) = d^J_{-M,-M'}(\theta) \tag{69}$$

Substituting θ→ $-\theta$

$$d^J_{M,M'}(\theta) = d^J_{M,M'}(-\theta) \tag{70}$$

2.1.3 LS Coupling Scheme

As previously shown, the spin orbit term is given by the equation 50 for one electron. In the energy regime when $H_{re} \gg H_{s-o}$ for more than one electron the spin orbit interaction is given by coupling the angular momentum and spin separately, and the coupling the total angular momentum and total spin[20]. For example, for two electrons will have:

$$H_{s-o} = \beta_1 \vec{l}_1 \vec{s}_1 + \beta_2 \vec{l}_2 \vec{s}_2 \tag{71}$$

In the LS-coupling scheme the orbital angular momenta of the two electrons couple to give total angular momentum $\vec{L} = \vec{l}_1 + \vec{l}_2$. In the vectormodel $\vec{l}_1$ and $\vec{l}_2$ precess around$\vec{L}$,similarly, $\vec{s}_1$ and $\vec{s}_2$ precess around $\vec{S}$,.
L and S precess around the total angular momentum J (but more slowly than the precession of$\vec{l}_1$and $\vec{l}_2$ around$\vec{L}$ because the spin–orbit interaction is "weaker" than the residual electrostatic interaction). Applying this procedure in equation 54:

$$H_{s-o} = \beta_1 \frac{\langle \vec{l}_1 \vec{L} \rangle}{L(L+1)} \vec{L} \frac{\langle \vec{s}_1 \vec{S} \rangle}{S(S+1)} \vec{S} + \beta_2 \frac{\langle \vec{l}_2 \vec{L} \rangle}{L(L+1)} \vec{L} \frac{\langle \vec{s}_2 \vec{S} \rangle}{S(S+1)} \vec{S} = \beta_{LS} \vec{L} \vec{S} \tag{58}$$

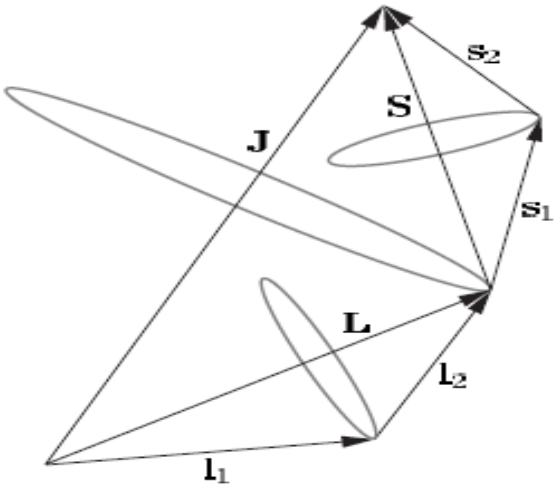

Figure 22:The JJ coupling scheme. When,$H_{re} \ll H_{s-o}$ illustrated in vector model

2.1.4 JJ Coupling Scheme

To calculate the fine structure in LS-Coupling scheme, the spin-orbit interaction is treated as a perturbation in a configuration L^{2s+1} . This treatment is valid when $H_{re} \gg H_{s-o}$which is generally true in light atoms. Where,$H_{re} = \sum_{i<j}^{N} \frac{e}{r_{ij}}^2$ is the electron-electron repulsion. The spin-orbit interaction increasing with the atomic number as:

In heavier atoms, when $H_{re} \ll H_{s-o}$, each valence electron acts on its own.

The residual electron-electron interaction acts as a perturbation on the jj-coupled levels; it causes the angular momenta of the electrons to be coupled to give total angular momentum J = j_1 + j_2 (as illustrated in Figure 15).

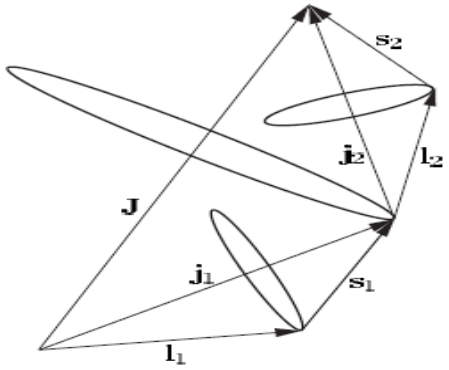

Figure 23: The JJ coupling scheme. When,$H_{re} \ll H_{s-o}$ illustrated in vector model.

The electron-electron interaction is calculated as:

$$\langle JM|A_{ee}\vec{j}_1\vec{j}_2|JM\rangle = \frac{A_{ee}}{2}\langle JM|J^2 - j_1^2 - j_2^2|JM\rangle = \frac{A_{ee}}{2}\{J(J+1) - j_1(j_1+1) - j_2(j_2+1)\} \quad (59)$$

2.2 Hyperfine structure

The interaction of μ_I,where $\mu_I = g_I\mu_N\vec{I}$ is the nuclear magnetic moment, $\mu_N = \mu_B/1836$, with the magnetic flux density created by the electrons, B_e gives the Hamiltonian of Hyperfine interaction:

$$H_{HFS} = -\mu_I B_e \quad (60)$$

This gives rise to hyperfine structure which, as its name suggests, is smaller than fine structure. Nevertheless, it is readily observable for

isotopes that have a nuclear spin (I≠ 0). In our experiments we suppose that the electrons, either in Hydrogen or in Deuterium, have angular momentum l=0. To calculate magnetic interactions, we need to consider an s-electron as a distribution of magnetization given by:

$$M = g_s \mu_B \vec{s} |\psi(r)|^2 \tag{61}$$

This corresponds to the total magnetic moment of the electron $-g_s \mu_B \vec{s}$ spread out so that each volume element d^3r has a fraction $\vec{s}|\psi(r)|^2 d^3r$. of the total. For s-electrons this distribution is spherically symmetric and surrounds the nucleus, as illustrated in Fig. 6.1. To calculate the field at r = 0 we shall use the result from classical electromagnetism [21].
This indicates that inside a uniformly magnetized sphere the magnetic flux density is:

$$B_e = \frac{2}{3} \mu_o M \tag{72}$$

Substituting eq. (60) to eq. (62) we have:

$$H_{HFS} = \frac{2}{3} \mu_o g_I \mu_N g_s \mu_B |\psi(r)|^2 \vec{I}\vec{s} = A_{HFS} \vec{I}\vec{s} \tag{73}$$

or generally

$$H_{HFS} = A_{HFS} \vec{I}\vec{J} = \frac{A_{HFS}}{2} [F(F+1) - J(J+1) - I(I+1)]$$

Example 1: Hydrogen in ground state.
The lowest level of the hydrogen atom is 1s $^2S_{1/2}$, i.e. J = 1/2 and the proton has spin I = 1/2 so that F = 0 and 1 and these hyperfine levels have energies:

$$E_{HFS} = \frac{A}{2}[F(F+1) - J(J+1) - I(I+1)] = \begin{cases} \frac{A}{4} & \text{For F=1} \\ -\frac{3A}{4} & \text{For F=0} \end{cases}$$

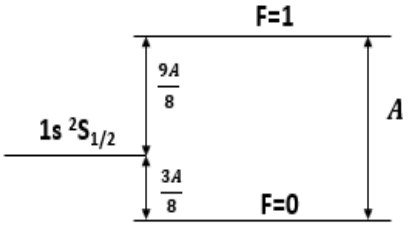

Figure 24: The splitting between the hyperfine levels in the ground state of hydrogen.

The $\Delta E_{HFS} = A_{HFS} = \frac{2}{3}\mu_o g_I \mu_N g_s \mu_B \frac{Z^3}{\pi \alpha_o^3 n^3}$[20].

Example 2: Deuterium in ground state.
The lowest level of the hydrogen atom is 1s $^2S_{1/2}$, i.e. J = 1/2 and the proton has spin I = 1 so that F = 3/2 and 1/2 and these hyperfine levels have energies:

$$E_{HFS}\frac{A}{2}[F(F+1)-J(J+1)-I(I+1)] = \begin{cases} \frac{9A}{8} & \text{For F=3/2} \\ -\frac{3A}{8} & \text{For F=3/2} \end{cases}$$

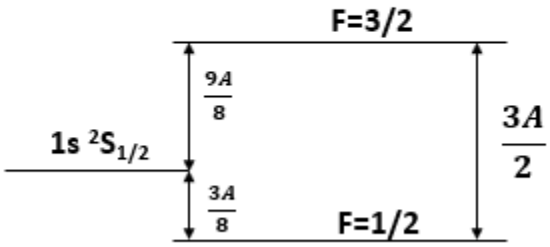

Figure 25 The splitting between the hyperfine levels in the ground state of deuterium

2.3 An Ultrafast, Spin-Polarized Hydrogen-based Magnetometer

A magnetometer is a device that measures magnetism—the direction, strength, or relative change of a magnetic field at a particular location. Magnetometers have a very diverse range of applications, including locating objects such as submarines, sunken ships, hazards for tunnel boring machines, hazards in coal mines, unexploded ordnance, toxic waste drums, as well as a wide range of mineral deposits and geological structures. They also have applications in heartbeat monitors, weapon systems positioning, sensors in anti-locking brakes, weather prediction (via solar cycles), steel pylons, drill guidance systems, archaeology, plate tectonics and radio wave propagation and planetary exploration and finally experimental particle physics to measure the magnetic field of pivotal components such as the concentration or focusing beam-magnets.

Depending on the application, magnetometers can be deployed in spacecraft, airplanes (fixed wing magnetometers), helicopters (stinger and bird), on the ground (backpack), towed at a distance behind

quad bikes (sled or trailer), lowered into boreholes (tool, probe or sonde) and towed behind boats (tow fish).

Typical magnetometers can operate down to ms timescales. whereas magnetometers based on nitrogen-vacancy centers in diamond can operate down to μs timescales [22]. However there are some phenomena such as: the measurement of surface magnetism [23], and the ultrafast generation of magnetic fields with short-pulse lasers [24], with applications in laser fusion, particle-beam generation, and laboratory astrophysics,where, nanosecond resolution is required. The SPA magnetometer that is presented below can measure in nanosecond timescale.

Spin polarized atoms (SPA) Magnetometer

SPA magnetometer measure magnetic field by using pulsed laser to directly polarize via photodissociation atoms. The quantum beating induced by the polarization transfer between the electron and nucleus is then detected via a pick-up coil, and an accurate measurement of the beating frequencies gives the magnitude and orientation of the magnetic field.

The major advantages of this method are: the ability of measuring magnetic fields with nanosecond time response, and the extremely high density of spin polarized atom up to 10^{19} atoms/cm^3.

More specifically, we use a 150 ps pulse-width laser (EKSPLA SL312M) which generates pulses 2.5 mJ at 213 nm at a 10 Hz repetition rate. The linearly polarized dissociation laser light is transmitted through a Photo-Elastic Modulator (Hinds Instruments PEM-90), which is synchronized with the laser using a custom-made frequency divider, so that the linear polarization is alternated from horizontal to vertical in each consecutive pulse. Subsequently, the laser light passes through a quarter-wave plate, in a way that the laser polarization switches from Right Circularly Polarized (RCP) to Left Circularly Polarized (LCP) in each consecutive pulse. Finally, the laser is focused, using an f = 100 mm lens, through and after the 2 mm diameter, 3.5 mm long, 4.5 turn pickup coil which detects the evolution of the magnetization of the H or D polarized atoms. The coil is placed in a vacuum chamber designed to withstand pressure up to 6 Bar, limited by the thickness

of our 6 mm windows, where the HCl and DCl are inserted. Finally, two permanent magnets are placed onto the chamber creating a homogeneous magnetic field perpendicular to the photodissociation axis. This process takes advantage of the symmetry between the two opposite signals created by the RCPP and LCPP. Therefore, with the subtraction of these two signals, most of the noise is cancelled out and also the signal is enhanced by a factor of 2.

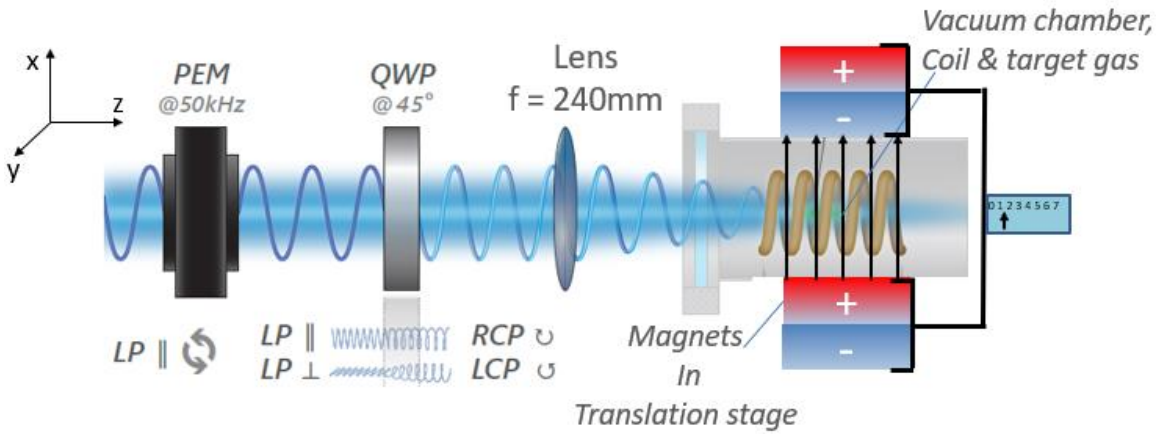

Figure 26:: Experimental schematic illustrating the laser beam path: the PEM alternates the laser linear polarization from vertical (LP$^{\perp}$) to horizontal (LP$\|$), and thus the quarter-waveplate (QWP) creates RCP and LCP on a shot-to-shot basis, which is focused into the coil inside the chamber in the presence of a modulating external magnetic field

2.4 Preparation of polarized atoms by photodissociation

The production of high-density polarized atoms by the photodissociation of diatomic molecules was proposed by van Brunt and Zare in 1968[11]. This technique exploits the fact that the projection of the molecular electronic angular momentum, for prompt photodissociation, is conserved within the atomic photofragments. In fact, the electronic states of diatomic molecules correlate adiabatically, at large internuclear separation, to atoms in specific |JM> states:

$$\mathrm{AB}(\Omega_i) \rightarrow A(J_A, M_A) + B(J_B, M_B) \qquad (63)$$

where AB is a diatomic molecule, Ω_i is the projection of the total electronic angular momentum of electronic state i along the AB bond axis, and (J_A, M_A) and (J_B,M_B) are the atomic states of atoms A and B, respectively.
Conservation of angular momentum projection along the recoil direction yields the important constraint:

$$\Omega_i = M_A + M_B \qquad (64)$$

In our experiment we examine the photodissociation of HCl by circularly polarized light. For example, the photodissociation of HCl molecules by circularly polarized light[25]. The absorption of left circularly polarized light (σ=-1) (propagating parallel to the HCl bond) by ground state HCl (Ω=0) produces excited state HCl with Ω=-1. In the dissociation step, the conservation of Ω between the photofragment angular momentum projections M_H and M_{Cl} produces polarized atoms.

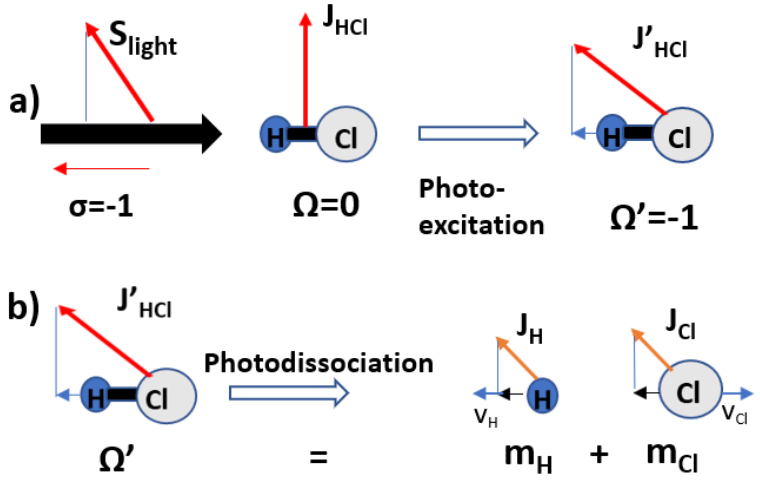

Figure 27a) Photo-excitation of HCl b) dissociation of HCl with circular polarized light.

Generally, the potential energy curves of the three lowest electronic states of HY that play a role in the photodissociation and photofragment polarization are shown in Fig. 28, A $^1\Pi_1$, $\alpha^3\Pi_1$, $\alpha^3\Pi_{0+}$ as well as the ground state $^1\Sigma_{0+}$ [25]These three states correlate adiabatically to the atomic m states as:

$$HY(A\,^1\Pi_1;\ \Omega=\pm1) \rightarrow H(m_H=\mp1/2) + Y(m_Y=\pm3/2) \qquad 65.a$$

$$HY(a\,^3\Pi_1;\ \Omega=\pm1) \rightarrow H(m_H=\pm1/2) + Y(m_Y=\pm1/2) \qquad 65.b$$

$$HY(a\,^3\Pi_{0+};\ \Omega=0) \rightarrow H(m_H=\pm1/2) + Y^*(m_Y=\mp1/2) \qquad 65.c$$

where Y refers to ground-state Y($^2P_{3/2}$) atoms, and Y* refers to spin-orbit-excited Y($^2P_{1/2}$) atoms. In order to achieve the maximum polarization, the molecular bonds can be aligned along the polarization direction of the photodissociation laser, using the method of strong-field laser alignment.

It is noteworthy that equations 65a, 65b describe the excitation of A $^1\Pi_1$ and $\alpha^3\Pi_1$ enables the production of SPH with spin down or up, respectively. Equation 65.c which yields unpolarized H atoms. The results of this equation could be avoided if the molecular bonds are aligned parallel to the polarization axis of the circularly polarized photodissociation laser. In addition, in all Hydrogen Halides, it is possible to excite, almost exclusively, the A $^1\Pi_1$state, or the $\alpha^3\Pi_1$state, with a large absorption cross section in the UV. Therefore, conditions do exist where the excitation step is fully compatible with the production of (near) 100% spin-polarized H atoms.

The strength and the main advantage of the idea is that the mechanism of production of the polarized atoms is a natural process (photodissociation) and does not require a complicated experimental preparation. Moreover, the density of the polarized atoms can be extremely high, approximately as high as the parent molecule density, which is much higher than that possible with most other techniques. It should be noted that maximum polarization (in the case of atomic orientation) is achieved only for recoil directions parallel to the quantization axis of the photolysis laser (i.e. the propagation direction), whereas the polarization of photofragments recoiling at an angle θ will be reduced by cosθ.

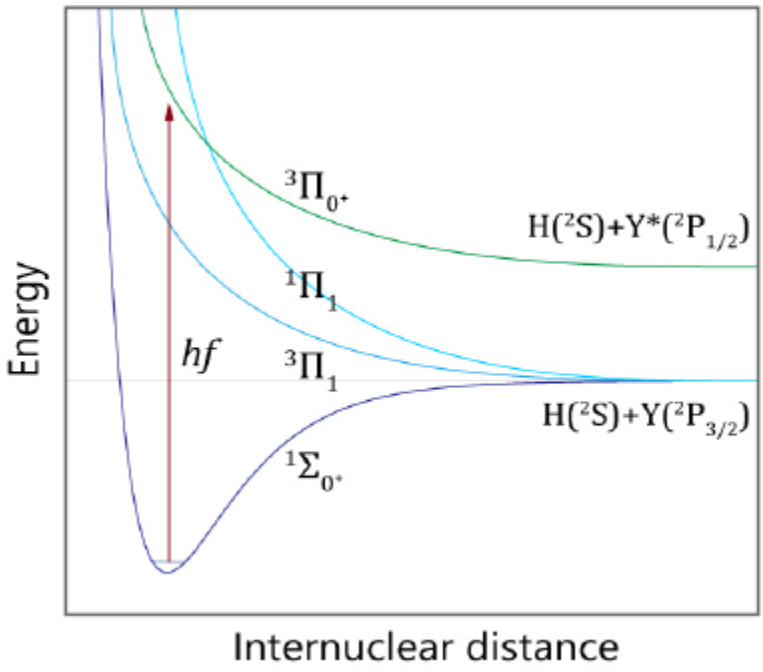

*Figure 28.*The potential energy curves that participate in the photodissociation HY.

2.5 Polarization transfer from molecular rotation to nuclear spin

In the previous decades, several studies have examined the preparation of aligned reagents produced by pulsed lasers. The initial polarization was found to oscillate due to nuclear spin, an explanation that led to predictions verified by experimental measurements for many molecular system.

The angular momentum entities associated with the electron J, L, S are usually weakly coupled to the one associated to the nuclei I via the hyperfine interaction, and are thus considered to be independent from each other over relatively short timescales. Upon optical excitation of molecules (where the process is done with no hyperfine resolution), the absorption process tends to align (or orient depending on the light being linearly or circularly polarized) the angular momentum J, leaving unaffected the nuclear spin I that the molecule possesses. This is a consequence of the weak coupling of these spins and the short duration of the excitation process compared to the precession rates of the spins. Spin will initially have a random spatial distribution. If the molecular rotation polarization is observed in subsequent times, it will be found to vary in an oscillating fashion.

This oscillation is caused by quantum beating phenomena that are responsible for polarization exchange between the electron and the nuclear spin in a sub-nanosecond timescale. The nature of this quantum beating is nothing else than a consequence of conservation of angular momentum and the result of the Schrödinger description of the time-dependent equation of a wavefunction. For example, by the photodissociation of HCl with RCPL (σ=1) or LCPL (σ=-1) we will have.

$$HCl(\Omega = 1) \rightarrow H(m_H = 1/2) + Cl(m_{Cl} = 1/2) \qquad (66)$$
$$HCl(\Omega = -1) \rightarrow H(m_H = -1/2) + Cl(m_{Cl} = -1/2)$$

Therefore, the electronic spin of Hydrogen will be ½ for the RCPL and -½ for the LCPL. As for the nuclear spin, which is not affected from the photodissociation, it is randomly distributed.

Those two angular momenta are coupled to form the total angular momentum state F which is the "good" quantum number of the system. The following picture shows the situation for S = I = ½.

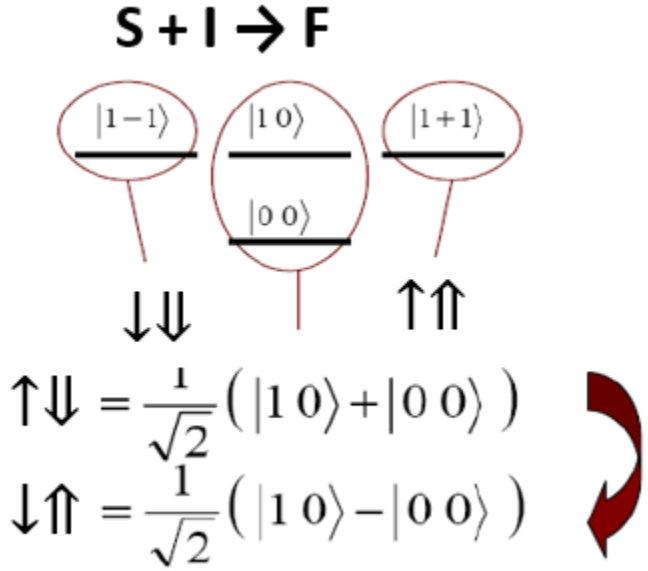

Figure 29. Total angular momentum states for an atom with S = I = ½. The co-oriented spins correspond to eigenstates of the system while the counter-oriented to superposition of total angular momentum states.

As we see in the figure, the co-oriented spins are eigenstates of the system while the counter-oriented are superpositions of them. Thus if the system is found in one of the counter-oriented spin states, it will be found in the other at later times and this situation will continue in a harmonic way with a period T=2πħ/ΔE, where ΔE is the energy difference between the eigenstates $|11\rangle$ and $|01\rangle$ as the eq.67 indicates.

$$|\uparrow\Downarrow\rangle = \frac{1}{\sqrt{2}}(|10\rangle + |00\rangle e^{i\Delta E t/\hbar})$$
$$|\downarrow\Uparrow\rangle = \frac{1}{\sqrt{2}}(|10\rangle - |00\rangle e^{i\Delta E t/\hbar}) \qquad (67)$$

2.6 Detection of Spin Polarized atoms

Samples with time-dependent polarization can be detected with a pick up coil, as in NMR. In our experimental set up, as described earlier, a pickup coil with ~4 turns, 5mm length and ~2 mm diameter, is placed in a small vacuum chamber. A 150-ps, 213-nm, circularly-polarized light pulse, passes through the coil, and photodissociates the molecules of the hydrogen halide gas, at typical pressures of about 1-5 bar. Inside the coil about

$10^{13} - 10^{14}$ Hydrogens are produced. The electrons of the Hydrogens are initially polarized with their spin up, whereas the polarization of the protons is random. The electron polarization is transferred to the protons and back, at the hyperfine beating frequency, as described in 2.6 section, Therefore, the electron magnetization M(t) is given by:

$$\mathrm{M(t)} = \mathrm{M_n e^{-t/\tau} cos^2(\frac{\Delta E t}{\hbar})} \tag{68}$$

where τ is the polarization lifetime, $\omega = (E_1 - E_0)/\hbar$ is the angular hyperfine frequency, E_F are the energies of the hyperfine states F = 0 and 1, $Mn = nP\mu_B n$ is the magnetization of n spin-polarized electrons with initial polarization P, and μ_B is the Bohr magneton. This time-dependent magnetization causes a time-dependent voltage in the coil.
The V(t) created in the coil is given by:

$$V(t) = \frac{dM(t)}{dt} - \frac{L}{R}\frac{dV(t)}{dt} \tag{69}$$

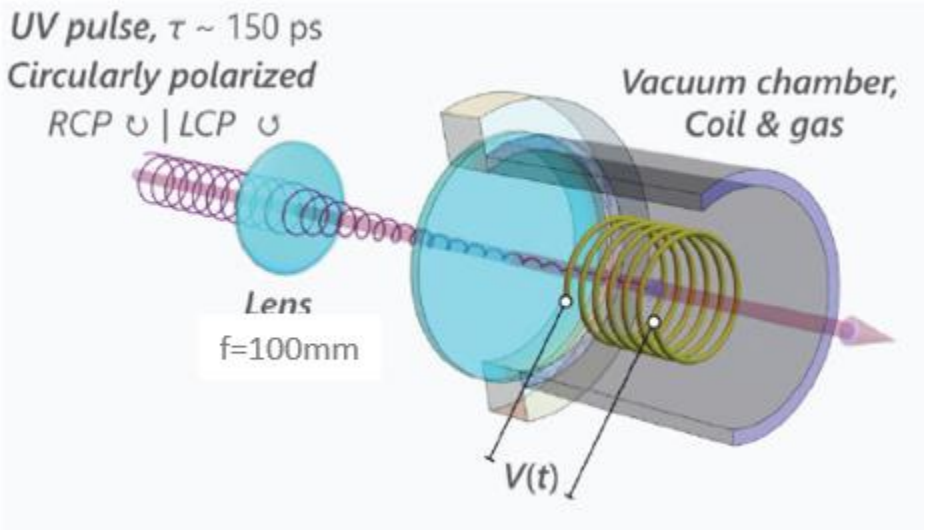

Figure 30:Detection scheme for SPH which consist of a pickup coil in the gas chamber that detects the time dependent Magnetization of the Hydrogens' electron.

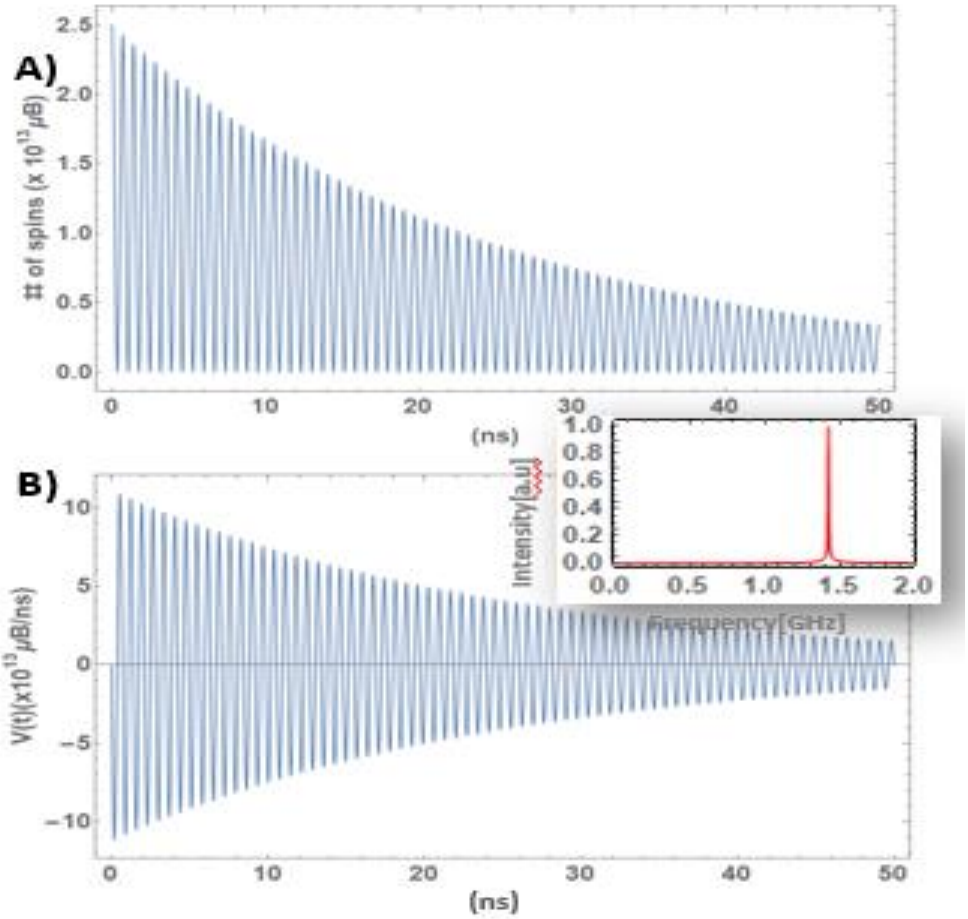

Figure 31: Time depended Magnetization B) Time depended Voltage (EMF) and its FFT.

Finally, the two EMF traces created by the RCPP and LCPP are subtracted taking advantage of the symmetry between the two opposite signals. Therefore, most of the noise is cancelled out and the signal is enhanced by a factor of 2.

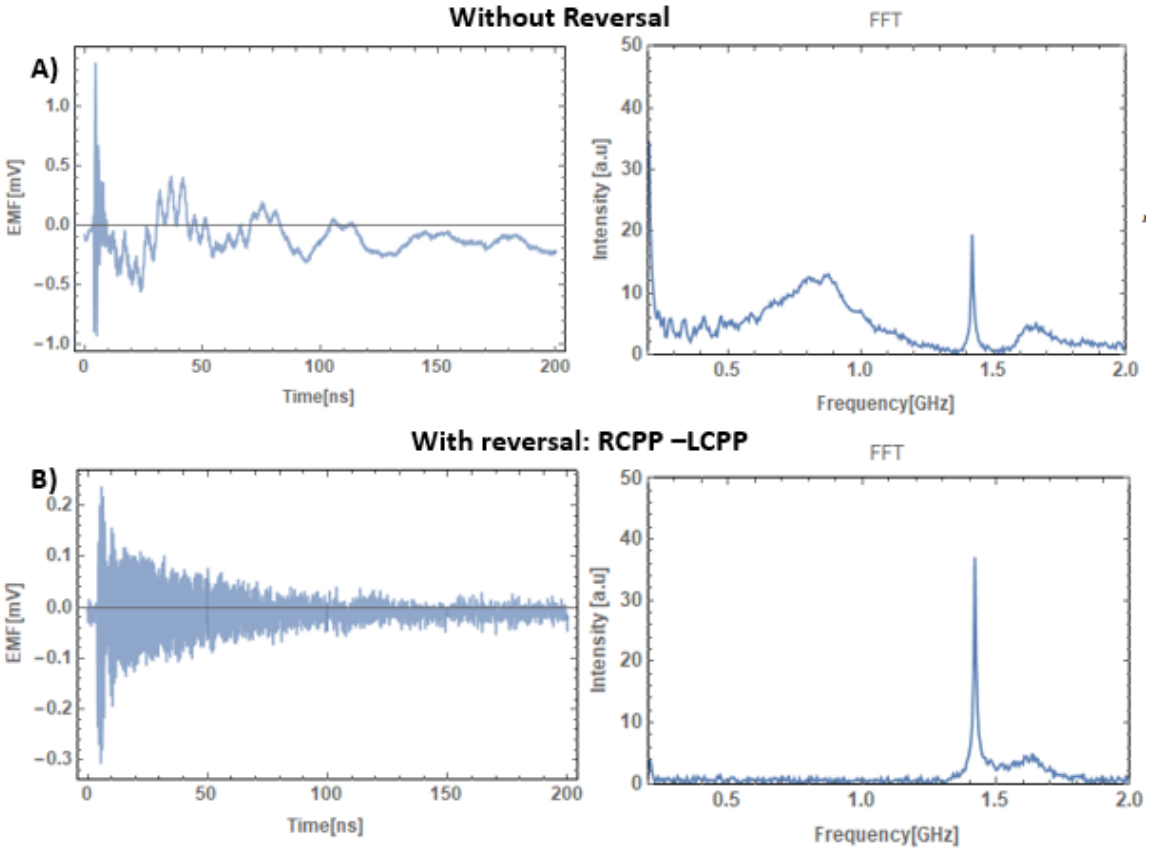

Figure 32. The EMF trace without Reversal, with only RCPL and its FFT, B) The EMF trace with Reversal, RCPL-LCPL and its FFT

2.7 Theoretical description of H in magnetic fields

The Hamiltonian that describes the physical system of the SPH magnetometer is:

$$\mathrm{H} = A_H \vec{I}\vec{J} + (\mu_B g_J \vec{J} + \mu_B g_I \vec{I})\vec{B} \tag{70}$$

or

$$\mathrm{H} = A_H I_z J_z + A_H I_x J_x + A_H I_y J_y + \mu_B g_J J_x B_x + \mu_B g_I \mathrm{I}_x B_x \tag{71}$$

Where, $A\vec{I}\vec{J}$ is the hyperfine interaction term and $(\mu_B g_J \vec{J} + \mu_B g_I \vec{I})\vec{B}$ is the Zeeman interaction of the magnetic moment of electron and proton with the external magnetic field. In addition, A_H is the hyperfine constant of hydrogen, and g_J ,g_I are the gyromagnetic constants of electron and hydrogen's nucleus respectively.

Regardless to figure 27, the external magnetic field (x-axis) is perpendicular to the direction of photodissociation(z-axis). By using the identity $J_+=J_x+iJ_y$ and $J_-=J_x- iJ_y$ the eq. 71 becomes:

$$\mathrm{H} = A_H I_z J_z + \frac{A_H I_+ J_+ + A_H I_- J_-}{2} + \mu_B g_J \frac{J_+ + J_-}{2} B_x + \mu_B g_I \frac{I_+ + I_-}{2} B_x \tag{72}$$

Therefore, the Hamiltonian matrix in the base $|M_I M_J\rangle$is:

$$\begin{array}{c} \\ |\uparrow\Uparrow\rangle \\ |\uparrow\Downarrow\rangle \\ |\uparrow\Uparrow\rangle \\ |\uparrow\Downarrow\rangle \end{array} \begin{array}{c} \begin{array}{cccc} |\uparrow\Uparrow\rangle & |\uparrow\Downarrow\rangle & |\uparrow\Uparrow\rangle & |\uparrow\Downarrow\rangle \end{array} \\ \begin{pmatrix} A_H/4 & \frac{B_x\mu_B g_J}{2} & 0 & \frac{B_x\mu_B g_I}{2} \\ \frac{B_x\mu_B g_J}{2} & -A_H/4 & \frac{B_x\mu_B g_I}{2} & A_H/2 \\ 0 & \frac{B_x\mu_B g_I}{2} & A_H/4 & \frac{B_x\mu_B g_J}{2} \\ \frac{B_x\mu_B g_I}{2} & A_H/2 & \frac{B_x\mu_B g_J}{2} & -A_H/4 \end{pmatrix} \end{array} \tag{73}$$

The double arrow refers to electron, and the single to the hydrogen's nucleus. The eigenvalues of the Hamiltonian are given by the analytical expressions:

$$E_1 = \frac{1}{4}(A + 2aB + 2bB) \tag{74}$$

$$E_2 = \frac{1}{4}(A - 2aB - 2bB)$$

$$E_3 = \frac{1}{4}(-A + 2\sqrt{A^2 + a^2B^2 - 2abB^2 + b^2B^2})$$

$$E_4 = \frac{1}{4}(-A - 2\sqrt{A^2 + a^2B^2 - 2abB^2 + b^2B^2})$$

Where, a=$\mu_B g_J$ and $b = \mu_B g_I$.

In accordance with section: 2.6, RCPL creates almost 100% polarized Hydrogens with electron spin "up" and LCPL with spin "down"[26]. The significant role of the coil is to detect the EMF trace which is created by the change in magnetization of polarized hydrogens' atoms. In other words, the

coil detects the average value of the spin of electrons in z-axis. In these calculations, we could neglect the change of magnetization due to nucleus, Since its magnetic moment is about 2000 times smaller than that of the electron. Thus, for RCPL the coil will detect:

$$\langle \mathrm{Sz} \rangle = \frac{d}{dt} \sum_{S,I=-1/2}^{S,I=1/2} \lambda |\langle I, 1/2^0 | \mathrm{I}, S^t \rangle|^2 \quad , \lambda = \pm 1/2 \text{ for } \mathrm{S} = \pm 1/2 \tag{75}$$

While for the LCPL:

$$\langle \mathrm{Sz} \rangle = \frac{d}{dt} \sum_{S,I=-1/2}^{S,I=1/2} \lambda |\langle I, -1/2 \Downarrow^0 | \mathrm{I}, S^t \rangle|^2 \quad , \lambda = \pm 1/2 \text{ for } \mathrm{S} = \pm 1/2 \tag{76}$$

Finally, the two traces are subtracted to cancel out the noise, thus we have:

$$\langle Sz_{tot} \rangle = \frac{d}{dt} \sum_{S,I=-1/2}^{S,I=1/2} \lambda |\langle I, 1/2^0 | \mathrm{I}, S^t \rangle|^2 - \frac{d}{dt} \sum_{S,I=-\frac{1}{2}}^{S,I=\frac{1}{2}} \lambda |\langle I, -1/2^0 | \mathrm{I}, S^t \rangle|^2 \tag{77}$$
$$\lambda = \pm 1/2 \text{ for } \mathrm{S} = \pm 1/2$$

Although, equation 77 describes the experiment totally and correctly, we have to take into account the physics of the experiment to understand which are the permitted changes in the projection of angular momentum as the system evolves in time. The answer to this question is given by the good quantum numbers from Ehrenfest theorem.

$$\frac{d\langle A(t) \rangle}{dt} = \langle \frac{\partial A(t)}{\partial t} \rangle + \frac{1}{i\hbar} \langle [H, A] \rangle \tag{78}$$

It is trivial to prove that the operators that commute with Hamiltonian and consequently their eigenvalues don't change in time are $F_+$and F_-. Thus, ΔMF= ± 1 as it is illustrated in figure

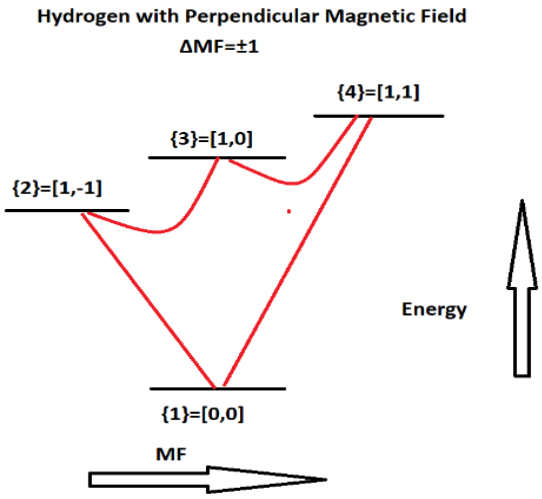

Figure 33: The permitted changes of MF as the system progresses in time, As a consequence of Ehrenfest theorem.

In the following figure the quantum beatings are represented as a function of magnetic field.

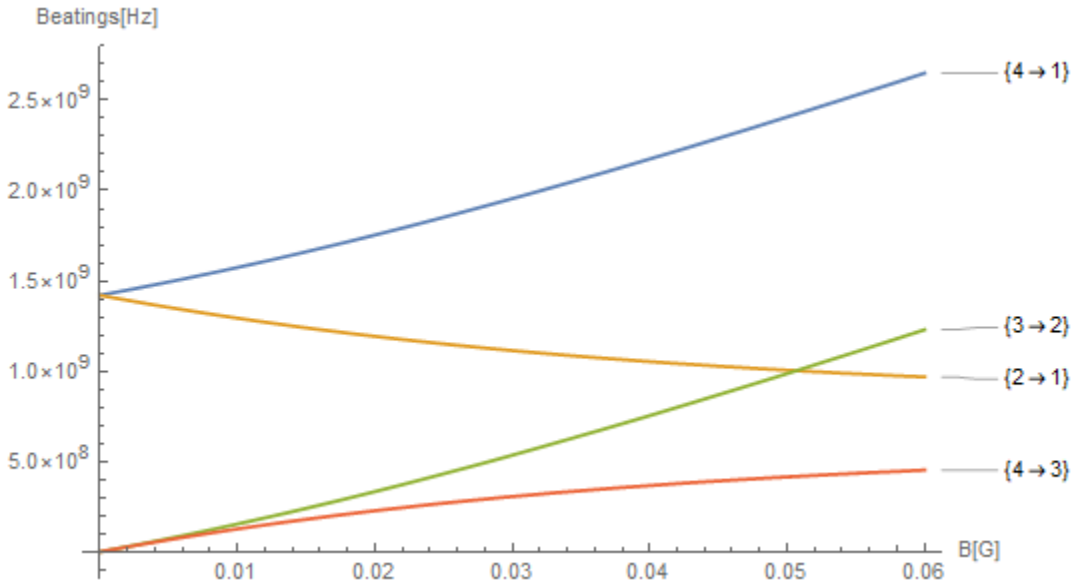

Figure 34 Quantum Beating [Hz] as a function of magnetic field [G].

Finally, analytical expressions for the base $|M_I M_J\rangle$ are derived by solving the Hamiltonian with setting the quantum axis of spin parallel to the magnetic field, where the Hamiltonian could be diagonalized.

The eigenvalues of the system are given by equation 74, and the eigenvectors are given by the following expressions

- $|1\rangle_z = |\uparrow\Uparrow\rangle_z$ (79)
- $|3\rangle_z = |\downarrow\Downarrow\rangle_z$
- $|2\rangle_z = |\downarrow\Uparrow\rangle_z \cos\theta + |\uparrow\Downarrow\rangle_z \sin\theta$
- $|4\rangle_z = |\uparrow\Downarrow\rangle_z \cos\theta - |\downarrow\Uparrow\rangle_z \sin\theta$

Where, $\tan 2\theta = \frac{B}{Bc}$, $Bc = 50.7mT$. Then, the $|M_I\rangle_z$, $\left|M_J\right\rangle_z$ are rotated 90º around the y-axis:

$$|\uparrow\rangle_x = \frac{1}{\sqrt{2}}\left(|\uparrow\rangle_z + |\downarrow\rangle_z\right) \text{ , } |\downarrow\rangle_x = \frac{1}{\sqrt{2}}\left(-|\uparrow\rangle_z + |\downarrow\rangle_z\right) \quad (80)$$
$$|\Uparrow\rangle_x = \frac{1}{\sqrt{2}}\left(|\Uparrow\rangle_z + |\Downarrow\rangle_z\right) \text{ , } |\Downarrow\rangle_x = \frac{1}{\sqrt{2}}\left(-|\Uparrow\rangle_z + |\Downarrow\rangle_z\right)$$

Then, we take the $|M_I\rangle_x \otimes |M_I\rangle_x$ and we substitute in equation 79:

- $|\uparrow\Uparrow\rangle_x = \frac{1}{2}|1\rangle_z + \frac{1}{2}|3\rangle_z + \frac{1}{2}\left(\cos\theta + \sin\theta\right)|2\rangle_z + \frac{1}{2}\left(\cos\theta - \sin\theta\right)|4\rangle_z$ (81)
- $|\uparrow\Downarrow\rangle_x = -\frac{1}{2}|1\rangle_z + \frac{1}{2}|3\rangle_z + \frac{1}{2}\left(\sin\theta - \cos\theta\right)|2\rangle_z + \frac{1}{2}\left(\cos\theta + \sin\theta\right)|4\rangle_z$
- $|\downarrow\Downarrow\rangle_x = \frac{1}{2}|1\rangle_z + \frac{1}{2}|3\rangle_z - \frac{1}{2}\left(\cos\theta + \sin\theta\right)|2\rangle_z + \frac{1}{2}\left(\sin\theta - \cos\theta\right)|4\rangle_z$
- $|\downarrow\Uparrow\rangle_x = -\frac{1}{2}|1\rangle_z + \frac{1}{2}|3\rangle_z + \frac{1}{2}\left(\cos\theta - \sin\theta\right)|2\rangle_z - \frac{1}{2}\left(\cos\theta + \sin\theta\right)|4\rangle_z$

Finally, a theoretical figure of quantum beating frequencies as a function of several random magnetic fields is demonstrated.

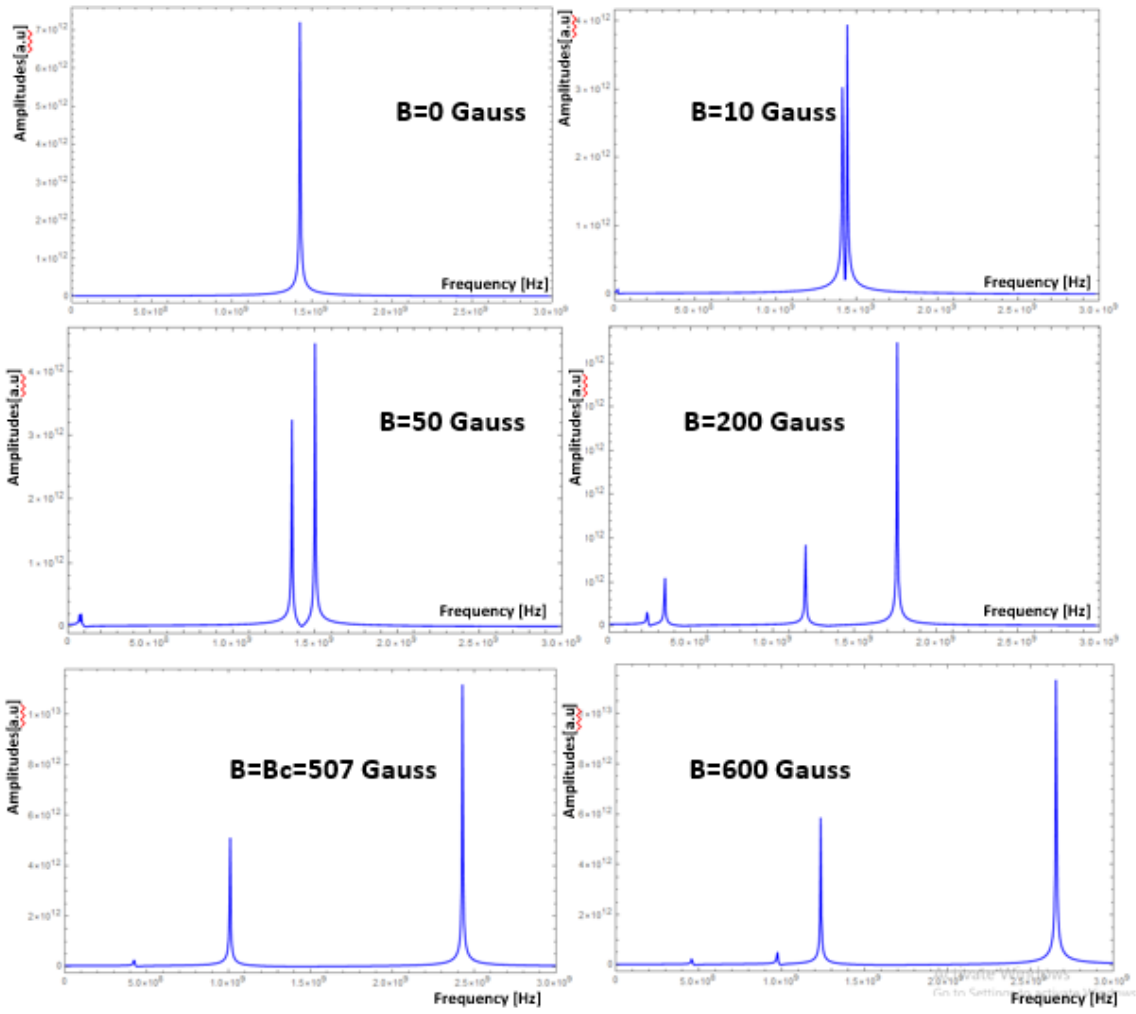

Figure 35 Quantum Beating [Hz] for several magnetic fields [G].

2.8 Theoretical description of D in magnetic fields

An alternative molecule that could be used with this technique as magnetometer is DCl The advantage of SPD in comparison to SPH is the nuclear spin of deuterium , which is 1. Therefore, SPD has more Fourier peaks. The Hamiltonian that describes the physical system of the SPD magnetometer is:

$$\mathrm{H} = A_D I_z J_z + \frac{A_D I_+ J_+ + A_D I_- J_-}{2} + \mu_B g_J \frac{J_+ + J_-}{2} B_x + \mu_B g_I \frac{I_+ + I_-}{2} B_x \tag{82}$$

By following, exactly the same procedure as in H the Hamiltonian matrix of D in the base $|M_I M_J\rangle$is:

$$\begin{array}{c} \\ |1\Uparrow\rangle \\ |1\Downarrow\rangle \\ |-1\Uparrow\rangle \\ |-1\Downarrow\rangle \\ |0\Downarrow\rangle \\ |0\Uparrow\rangle \end{array} \begin{array}{c} \begin{array}{cccccc} (|1\Uparrow\rangle & |1\Downarrow\rangle & |-1\Uparrow\rangle & |-1\Downarrow\rangle & |0\Downarrow\rangle & |0\Uparrow\rangle) \end{array} \\ \begin{pmatrix} \frac{A_D}{2} & \frac{B_x\mu_B g_J}{2} & 0 & 0 & 0 & \frac{B_x\mu_B g_I}{2} \\ \frac{B_x\mu_B g_J}{2} & -\frac{A_D}{2} & 0 & 0 & \frac{B_x\mu_B g_I}{\sqrt{2}} & \frac{A_D}{\sqrt{2}} \\ 0 & 0 & -\frac{A_D}{2} & \frac{B_x\mu_B g_J}{2} & \frac{A_D}{\sqrt{2}} & \frac{B_x\mu_B g_I}{\sqrt{2}} \\ 0 & 0 & \frac{B_x\mu_B g_J}{2} & \frac{A_D}{\sqrt{2}} & \frac{B_x\mu_B g_I}{\sqrt{2}} & 0 \\ 0 & \frac{B_x\mu_B g_I}{\sqrt{2}} & \frac{A_D}{\sqrt{2}} & \frac{B_x\mu_B g_I}{\sqrt{2}} & 0 & \frac{B_x\mu_B g_J}{2} \\ \frac{B_x\mu_B g_I}{\sqrt{2}} & \frac{A_D}{\sqrt{2}} & \frac{B_x\mu_B g_I}{\sqrt{2}} & 0 & \frac{B_x\mu_B g_J}{2} & 0 \end{pmatrix} \end{array} \quad (83)$$

The double arrow refers to electron and the 1,0, -1 to the hydrogen's nuclear. The eigenvalues of the Hamiltonian are given by the analytical expressions:

$$\begin{aligned} E_1 &= \frac{1}{2}(A + 2aB + 2bB) \\ E_2 &= \frac{1}{2}(A - 2aB - 2bB) \\ E_3 &= \frac{1}{4}\left(-A + 2bB + \sqrt{9A^2 + 4A\mathrm{a}\mathrm{B} - 4A\mathrm{b}\mathrm{B} + 4a^2B^2 + 4b^2B^2 - 8abB^2}\right) \\ E_4 &= \frac{1}{4}(-A + 2bB - \sqrt{9A^2 + 4A\mathrm{a}\mathrm{B} - 4A\mathrm{b}\mathrm{B} + 4a^2B^2 + 4b^2B^2 - 8abB^2}) \\ E_5 &= \frac{1}{4}(-A - 2bB + \sqrt{9A^2 - 4A\mathrm{a}\mathrm{B} + 4A\mathrm{b}\mathrm{B} + 4a^2B^2 + 4b^2B^2 - 8abB^2}) \\ E_6 &= \frac{1}{4}(-A - 2bB - \sqrt{9A^2 - 4A\mathrm{a}\mathrm{B} + 4A\mathrm{b}\mathrm{B} + 4a^2B^2 + 4b^2B^2 - 8ab\,B^2}) \end{aligned} \quad (84)$$

The coil will detect an EMF trace, which is defined as the average values of electron spin in z-axis and it is given by:

$$\langle Sz_{tot}\rangle = \frac{d}{dt}\sum_{I=-1}^{I=1}\sum_{S=-1/2}^{S=1/2}\lambda\left|\left\langle I,\frac{1}{2}^0\middle|\mathrm{I},S^t\right\rangle\right|^2 - \frac{d}{dt}\sum_{I=-1}^{I=1}\sum_{S=-\frac{1}{2}}^{S=\frac{1}{2}}\lambda|\langle I,-1/2^0|\mathrm{I},S^t\rangle|^2 \quad (85)$$

,$\lambda = \pm 1/2$ for S$= \pm 1/2$

By following, exactly the same procedure as in Hydrogen, the Ehrenfest theorem gives $F_+$and F_- as good quantum numbers. It can be also expressed as $\Delta m_{\mathrm{F}} = \pm 1$ as it is illustrated in figure 37.

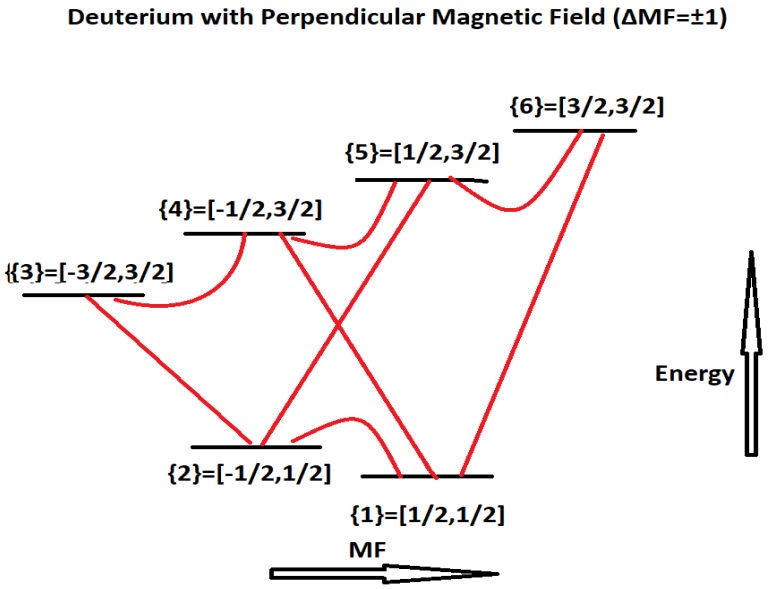

Figure 36:The permitted changes of MF as the system progresses in time, as a consequence of Ehrenfest theorem.

In the following figure the quantum beatings as a function of magnetic field are presented:

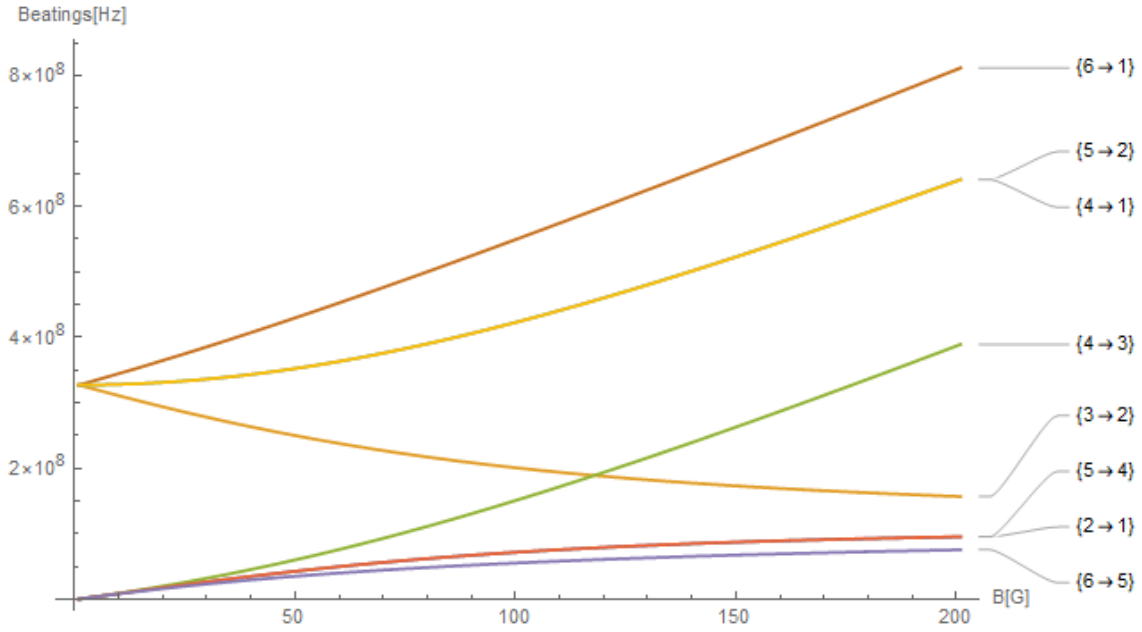

Figure 37: Quantum Beating [Hz] as a function of magnetic field [G].

Magnetic Field Parallel to Photodissociation axis

An alternative way to measure magnetic fields with SPD is to put an external magnetic field parallel to the photodissociation axis. In this situation the Hamiltonian and the Hamiltonian matrix is given by equation

$$\mathrm{HD}_{par} = A_D I_z J_z + \frac{A_D I_+ J_+ + A_D I_- J_-}{2} + \mu_B g_J J_z B_z + \mu_B g_I I_z B_z \tag{86}$$

$$(|1\Uparrow\rangle|1\Downarrow\rangle|-1\Uparrow\rangle|-1\Downarrow\rangle|0\Downarrow\rangle|0\Uparrow\rangle) \tag{87}$$

$$\begin{pmatrix} |1\Uparrow\rangle \\ |1\Downarrow\rangle \\ |-1\Uparrow\rangle \\ |-1\Downarrow\rangle \\ |0\Downarrow\rangle \\ |0\Uparrow\rangle \end{pmatrix} \begin{pmatrix} \frac{\mathrm{A_D}}{2}+\left(\frac{\mathrm{a}}{2}+b\right)B & 0 & 0 & 0 & 0 & 0 \\ 0 & -\frac{\mathrm{A_D}}{2}+\left(-\frac{\mathrm{a}}{2}+b\right)B & 0 & 0 & 0 & \frac{\mathrm{A_D}}{\sqrt{2}} \\ 0 & 0 & -\frac{\mathrm{A_D}}{2}+\left(\frac{\mathrm{a}}{2}+b\right)B & 0 & \frac{\mathrm{A_D}}{\sqrt{2}} & 0 \\ 0 & 0 & 0 & -\frac{\mathrm{A_D}}{2}+\left(\frac{\mathrm{a}}{2}+b\right)B & 0 & 0 \\ 0 & 0 & \frac{\mathrm{A_D}}{\sqrt{2}} & 0 & \frac{\mathrm{B_x}\mu_\mathrm{B}\mathrm{g_J}}{2} & 0 \\ 0 & \frac{\mathrm{A_D}}{\sqrt{2}} & 0 & 0 & 0 & \frac{\mathrm{B_x}\mu_\mathrm{B}\mathrm{g_J}}{2} \end{pmatrix}$$

The eigenvalues of the Hamiltonian are given by eq.84 and from the Ehrenfest theorem: $[\mathrm{HD}_{par},\mathrm{F}_z] = 0$ is deduced that $\Delta\mathrm{MF} = 0$. The permitted changes in ΔMF are depicted in figure below:

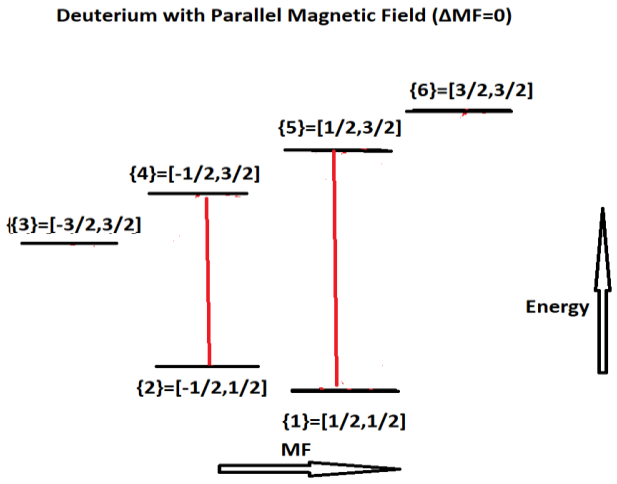

Figure 38 : The permitted changes of MF as the system progresses in time, as a consequence of Ehrenfest theorem.

In the following figure the quantum beatings as a function of magnetic field are presented:

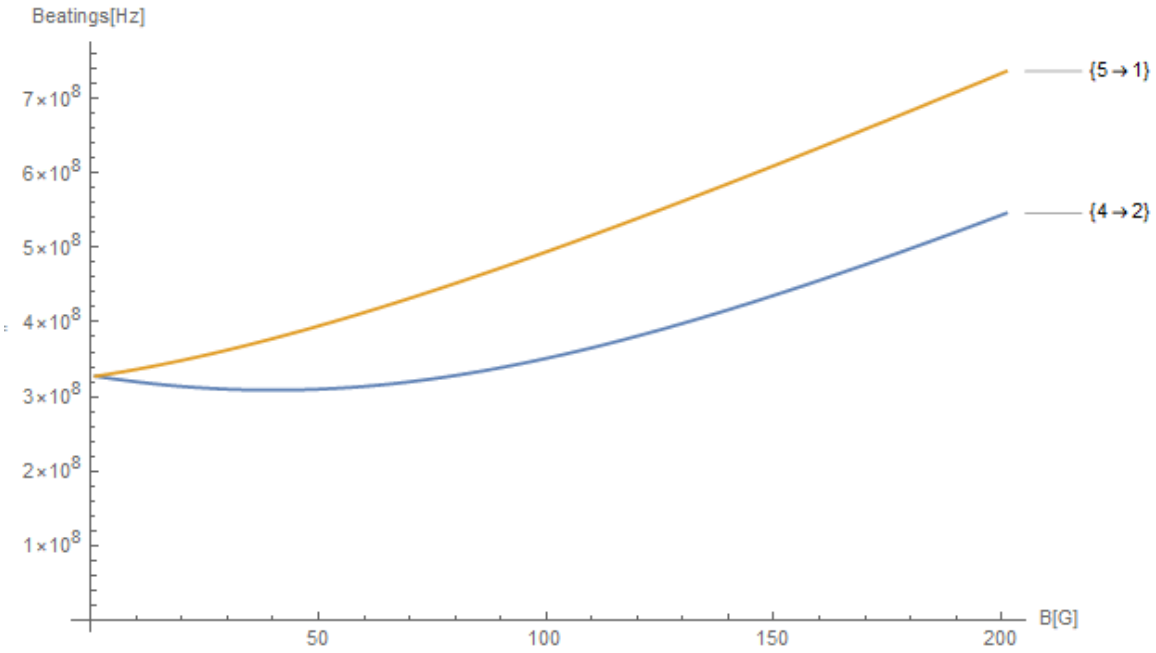

Figure 39: Quantum Beating [Hz] as a function of magnetic field [G].

2.9 Results and Discussion

As is extensively described in previous sections a gas of HCl at 2 Bar is placed in a vacuum chamber and is photodissociated by a 150 ps circularly polarized pulse at 213nm. The spin-polarized Hydrogens produce a time depended magnetization, and, as a consequence, an EMF signal, which is detected by the pickup coil.

Study for the optical gas pressure

The fundamental sensitivity of the atomic magnetometers is proportional to: $\delta \mathrm{B} \sim \frac{1}{\gamma}\sqrt{\frac{R_{tot}}{F_z \mathrm{N}}}$,where is the gyromagnetic ratio of the electron, N the number of spin polarized Hydrogens, R_{tot} is the depolarization rate. Based on the formula above the Number of SPHs, the number density of SPHs and the relaxation rate were calculated as it is depicted in figures 40-42.

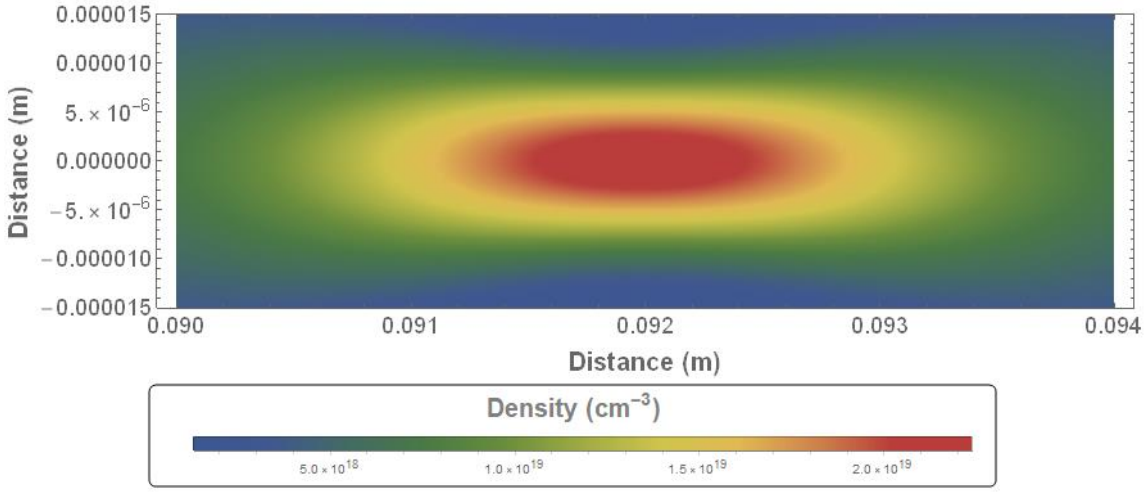

Figure 40: Number density of SPHs acquired with f=10cm and 2.5mJ pulse as a function of distance of the focal length.

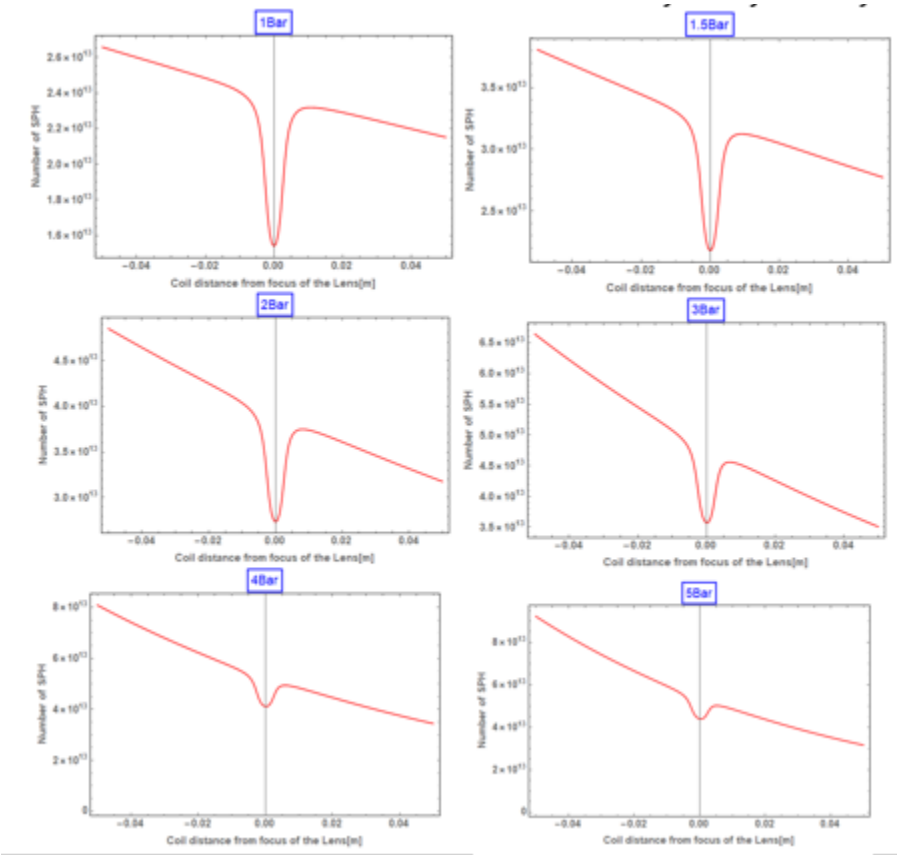

Figure 41: Number of SPHs, produced with f=10cm and 2.5mJ energy pulse, as a fuction of distance from the focal leangth.

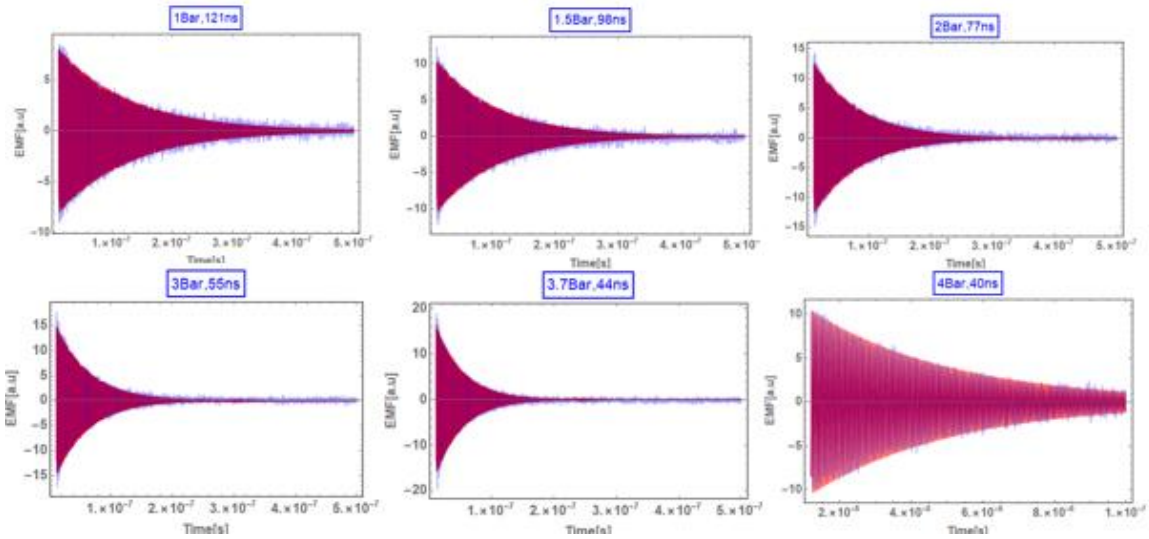

Figure 42: Relaxation time of SPH atoms as a function of gas pressure placed in the vacuum chamber

Finally, the results of this study, are aggregated in the next figure:

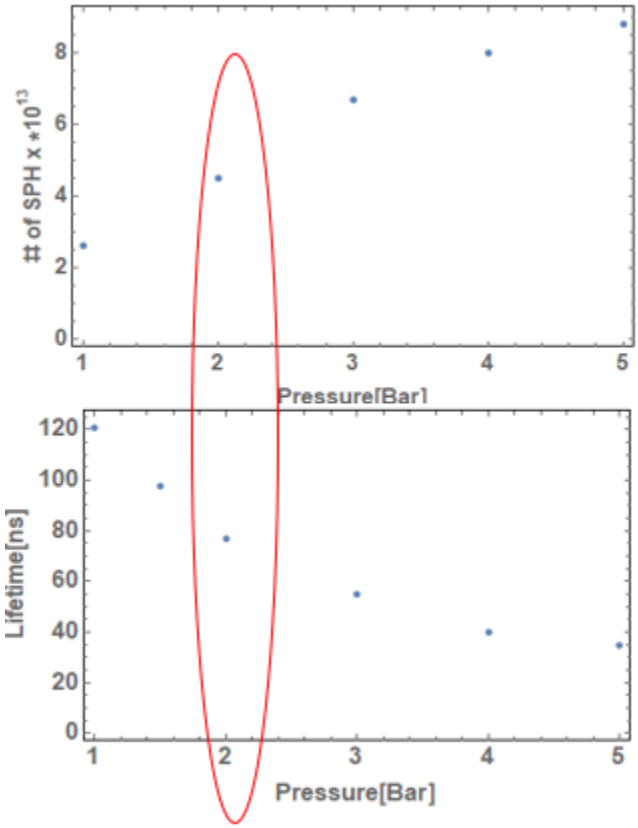

As a result, the optical gas pressure for the magnetometry experiments, regarding to sensitivity is found to be 2 bars.

The results of the magnetometry experiments are presented below:

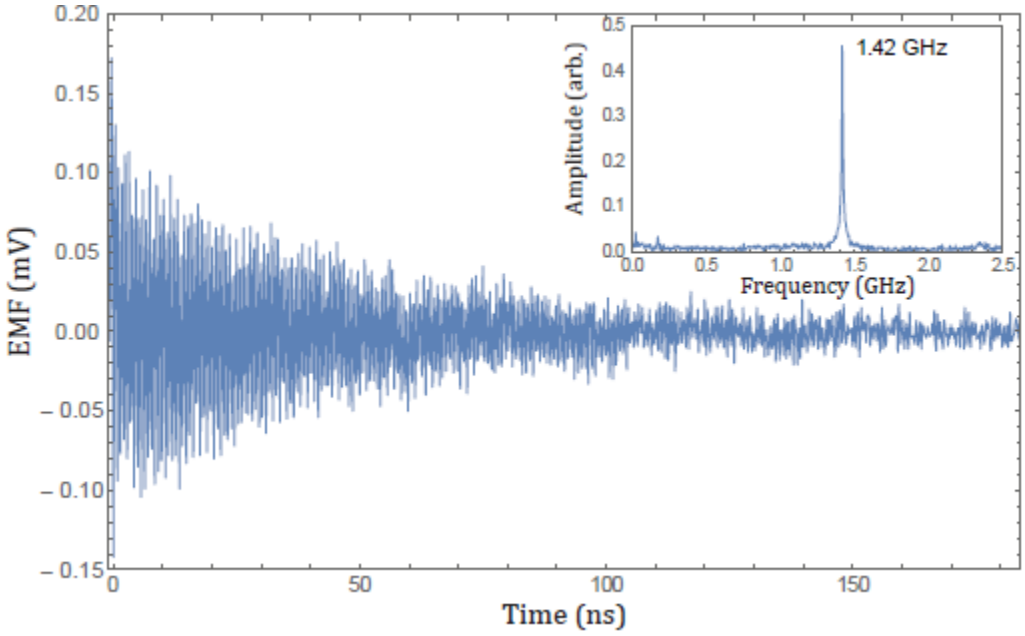

Figure 43: Experimental trace and FFT (inset) of the magnetization beating of SPH atoms from the photodissociation of 3.5 bar of HCl gas

Subsequently, two magnet plates are placed with their magnetization axis perpendicular to the photodissociation axis. The magnets are placed on a translation stage; thus, we are able to vary their distance between 1cm and 5cm, which is translated into (11-170) G. The smallest change in the magnetic field that we were able to produce with these translation stages was about 0.03 G and it is successfully detected by the coil. The measurements are exhibited below:

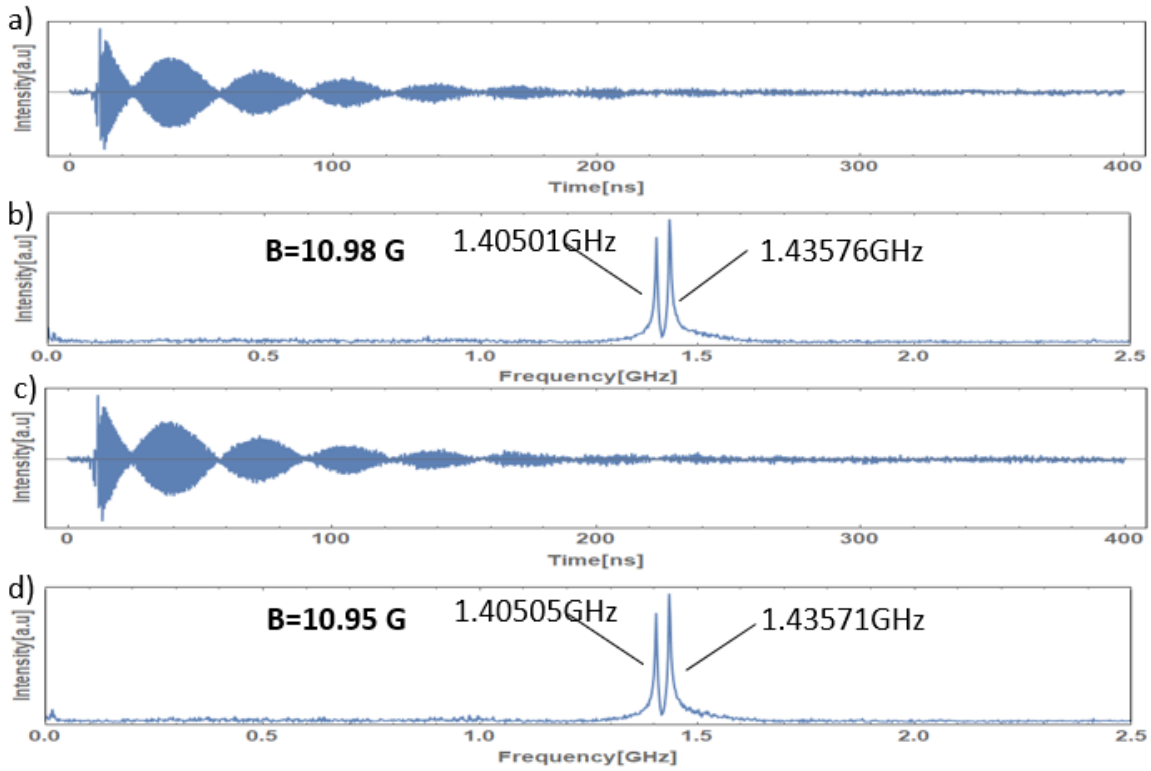

Figure 44: A) EMF(t) for magnetic field B=10.95 G. B) FFT of magnetic field 10.95 G. C) EMF(t) for magnetic field B=10.98 G. D) FFT of magnetic field 10.98 G.

In the next graph measurements for low magnetic fields (between 11 and 35 G) are presented. In this magnetic field range, only the two peaks at higher frequencies, *4→1 and 2→1 ,* are strong enough to be clearly

detected.

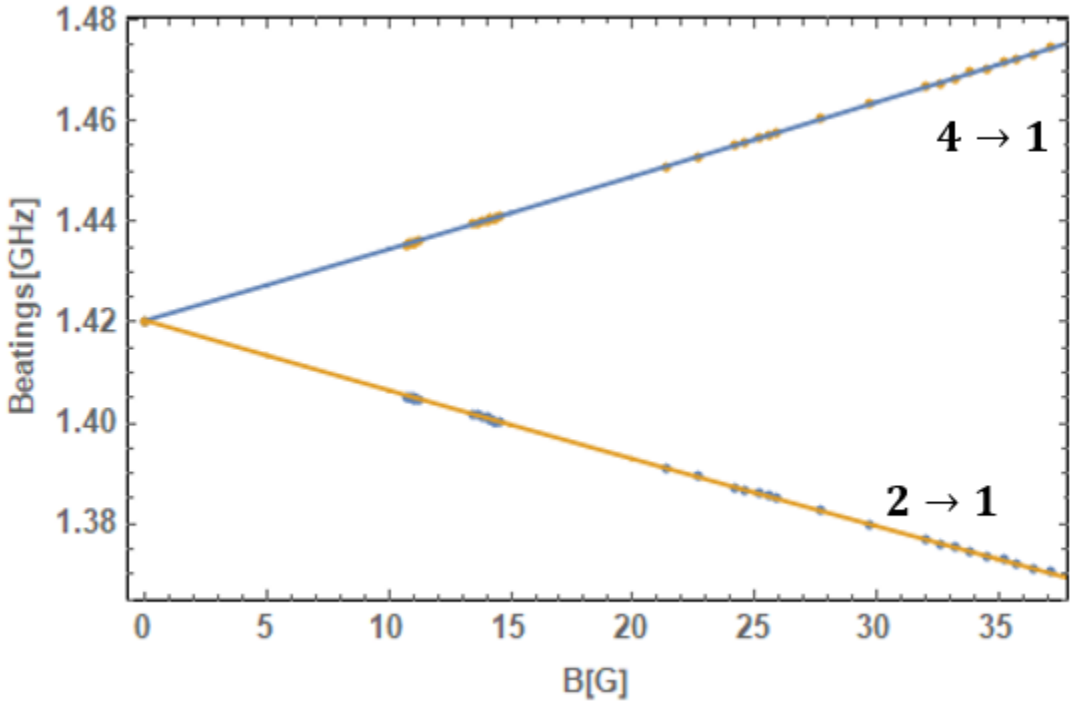

Figure 45: Quantum beating frequencies as a function of Magnetic field from B=11-35G.

As the magnets get closer, the magnetic field becomes larger, thus the two smaller peaks 3→2 and 4→3 show up. A typical EMF trace and its FFT are presented below.

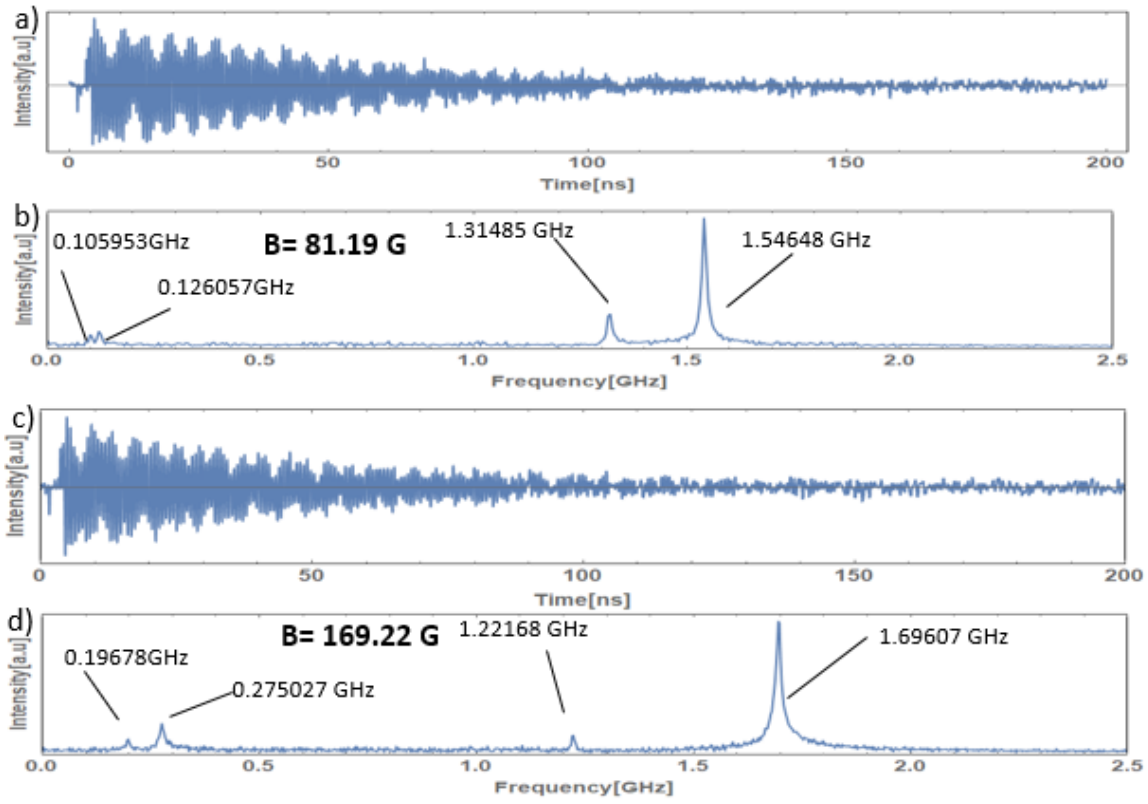

Figure 46:a) EMF(t) for magnetic field B=81.19 G. b) FFT of magnetic field 18.4G all four peaks are come up. :a) EMF(t) for magnetic field B=184.2 G. b) FFT of magnetic field 169.22 G all four peaks are come up and the splitting is larger as the theory predicts

In the next graph, measurements for low magnetic field between (75-90) G and (140-175)G are presented, where all four peaks 4→1 ,2→1,3→2,4→3 are clearly detected.

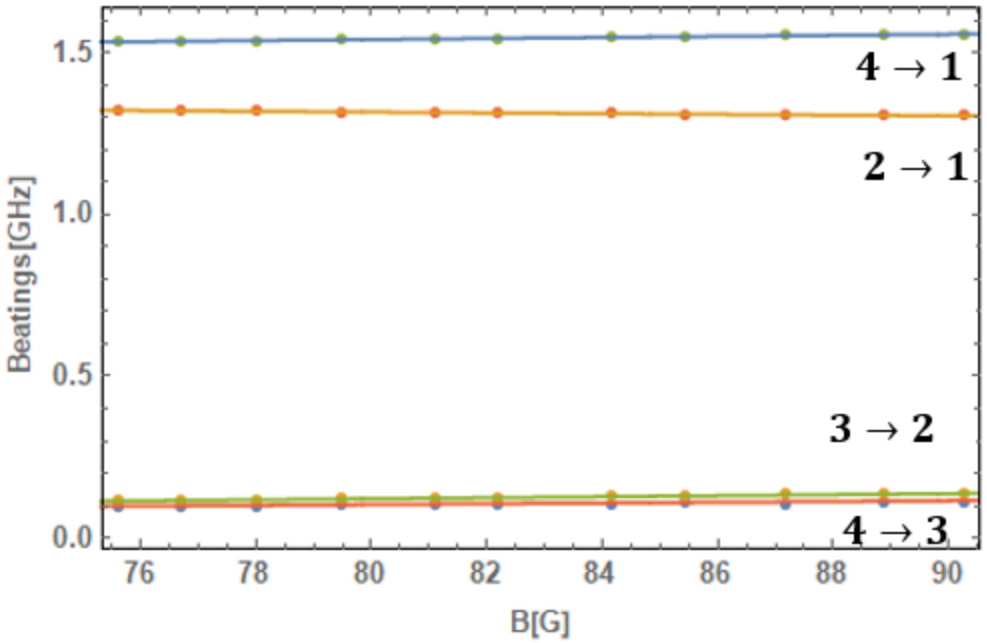

Figure 47: Quantum beating frequencies as a function of Magnetic field from B=70-90G

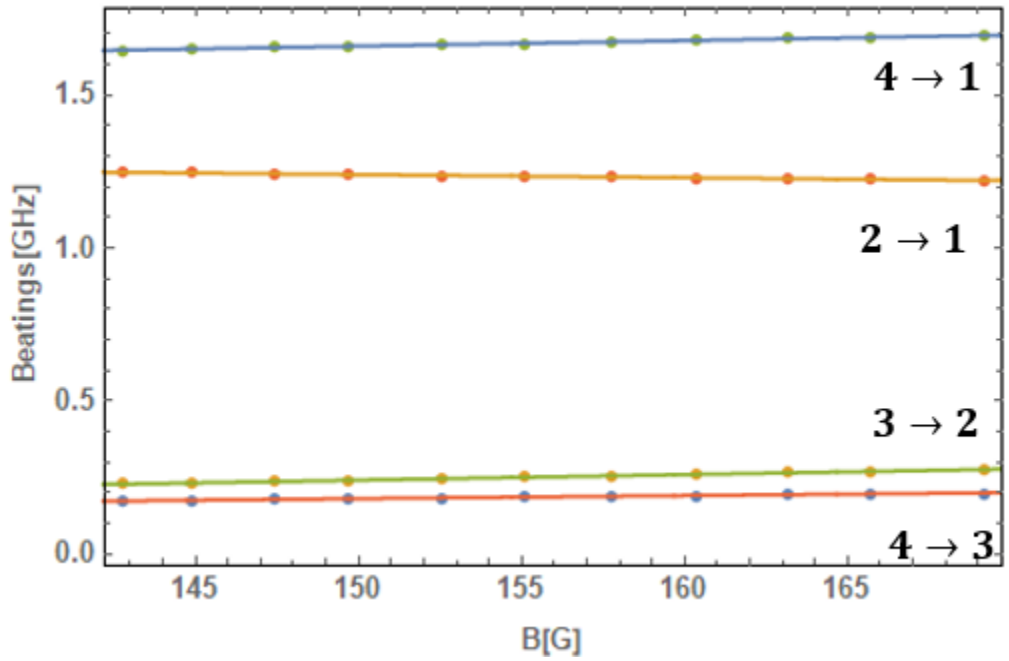

Figure 48: Frequencies of Quantum beating frequencies as a function of Magnetic field from B=140-165G

In conclusion, the experimental set-up we propose before (in this study) actually works as a magnetometer, which is capable in operating in a large magnetic field range. In addition, it can detect small changes of the magnetic field (at least 0.03G) within a few nanoseconds. However, there

are many factors that should be examined to make it more efficient. Moreover, a magnetic shield could protect the measurements from unexpected drifts and noises. Least but last, a laser with a higher intensity or repetition rate could help improve the sensitivity and speed of the measurements.

Appendix A

The code in Mathematica that is used for calculating the Quantum beating frequencies in Hydrogen as a function of magnetic field (figure 35) and the simulation of the Fourier transform of the exponential decay of the average value of the spin of electrons in z-axis due to depolarization from collisions, (figure 30).

Code

```
(Call the packet Quantum notation to use Dirac symbolism)
Needs ["Quantum` Notation`"];
SetQuantumAliases [];
(Defining some constants)
$Assumptions=t∈ Reals;
hbar=1.054571817*10-34;
AH=hbar* 2π *1420405751.7667; (Hyperfine term of H)
mb=-9.274009994*10-24 (Bohr magneton);
me=2* mb ;( Electron magnetic moment)
mnH=(5.6*mb)/1836;( Hydrogen nucleus magnetic moment)
MaxB=0.2;
pulsetime=2*10-7; (Measurement Time)
resolution=10-10;( Time Resolution)
(Defining the Hamiltonian of Hydrogen with normal magnetic field to the photodissociation axis)
```

HamiltonianH[B_]:

$$= \{\{A/4, \frac{a}{2}B, 0, \frac{b}{2}B\}, \{\frac{a}{2}B, -A/4, \frac{b}{2}B, A/2\}, \{0, \frac{b}{2}B, A/4, \frac{a}{2}B\}, \{\frac{b}{2}B, A/2, \frac{a}{2}B, -A/4\}\}$$

(Finding the eigenvalues and eigenvectors of the Hamiltonian above and sort the eigenvalues by increasing order.)

```
eigensys[B_]:=Eigensystem[HamiltonianH[B]/.{A→AH,a→me,b→mnH}];
esys2[B_]:= Partition[Riffle[eigensys[B][[1]],eigensys[B][[2]]],2];
esys[B_]: =Sort [Sort[esys2[B], #[[1]]<#[[2]] &]];
evals[B_]:=esys[B][[All,1]];
```

(Put the eigenvectors in a table and then transverse it)

ω[B_]:=1/hbar*esys[B][[All,1]];

$f[\text{B\_}]:=\frac{1}{2\pi\text{hbar}}\text{Sort}[\text{Eigenvalues}[\text{HamiltonianH}[B]/.\{A\to \text{AH}, a\to \text{me}, b\to \text{mnH}\}]];$

evecs[B_]:=esys[B][[All,2]];

States[B_]:=Table[evecs[B][[i]],{i,1,4}];

transstates[B_]:=Transpose[States[B]];

By employing the equations $|JM\rangle=\sum_{m_1m_2}C(j_1j_2;m_1m_2)|j_1m_1\rangle|j_2m_2\rangle$ or equivalently $|j_1m_1\rangle|j_2m_2\rangle=\sum_{J,M}C(j_1j_2;m_1m_2)\,|JM\rangle$ and $C(j_1j_2;m_1m_2)\equiv\langle j_1m_1j_2m_2|JM\rangle$ we express the eigenvectors for random Magnetic field as a function of $|M_S,M_I\rangle$:

$\text{procH[B\_]}:=\text{Module}[\{\text{bf}=B\},$

$\langle\psi_{\text{l}}|\psi_{\text{lpr\_}}\rangle:=\text{KroneckerDelta}[l,\text{lpr}]$

$\text{stateold[bf]}:=\text{Table}[\text{Sum}[\text{transstates}[B][[k]][[i]]|\psi_i\rangle\text{Exp}[-I\omega[\text{bf}][[i]]t],\{i,1,4\}],\{k,1,4\}];$

$\text{stateoldinit[bf]}:=\text{Table}[\text{Sum}[\text{transstates}[B][[k]][[i]]|\psi_i\rangle//\text{Chop},\{i,1,4\}],\{k,1,4\}];$

$|\text{upup0}\rangle=\text{stateoldinit[bf]}[[1]];(|\uparrow\uparrow,t=0\rangle)$

$|\text{updown0}\rangle=\text{stateoldinit[bf]}[[2]];(|\uparrow\downarrow,t=0\rangle)$

$|\text{downdown0}\rangle=\text{stateoldinit[bf]}[[3]];(|\downarrow\downarrow,t=0\rangle)$

$|\text{downup0}\rangle=\text{stateoldinit[bf]}[[4]];(|\downarrow\uparrow,t=0\rangle)$

$|\text{upup}\rangle=\text{stateold[bf]}[[1]];(|\uparrow\uparrow,t\rangle)$

$|\text{updown}\rangle=\text{stateold[bf]}[[2]];(|\uparrow\downarrow,t\rangle)$

$|\text{downdown}\rangle=\text{stateold[bf]}[[3]];(|\downarrow\downarrow,t\rangle)$

$|\text{downup}\rangle=\text{stateold[bf]}[[4]];(|\downarrow\uparrow,t\rangle)$

(Employing equation 67)

$\text{f1}=D[((((\langle\text{upup0}|\text{upup}\rangle\langle\text{upup}|\text{upup0}\rangle-\langle\text{updown0}|\text{upup}\rangle\langle\text{upup}|\text{updown0}\rangle)))$

$\text{Exp}[-2*t/\text{pulsetime}]/.t^*\to t)//\text{FullSimplify},t]//\text{Expand};$

$\text{f2}=D[((((\langle\text{upup0}/\text{downup}\rangle\langle\text{downup}/\text{upup0}\rangle-\langle\text{updown0}/\text{downup}\rangle\langle\text{downup}/\text{updown0}\rangle)))$

$\text{Exp}[-2*t/\text{pulsetime}]/.t^*\to t)//\text{FullSimplify},t]//\text{Expand};$

$\text{f3}=-D[((((\langle\text{upup0}/\text{updown}\rangle\langle\text{updown}/\text{upup0}\rangle-\langle\text{updown0}/\text{updown}\rangle\langle\text{updown}/\text{updown0}\rangle)))$

$\text{Exp}[-2*t/\text{pulsetime}]/.t^*\to t)//\text{FullSimplify},t]//\text{Expand};$

```
f4 = −D[((((⟨upup0/downdown⟩⟨downdown/upup0⟩
        − ⟨updown0/downdown⟩⟨downdown/updown0⟩)))

Exp[−2 ∗ t/pulsetime]/. t* → t)//FullSimplify, t]//Expand;

f5 = D[((((⟨downup0/upup⟩⟨upup/downup0⟩ − ⟨downdown0/upup⟩⟨upup/downdown0⟩)))

Exp[−2 ∗ t/pulsetime]/. t* → t)//FullSimplify, t]//Expand;


f6 = D[((((⟨downup0|downup⟩⟨downup|downup0⟩
        − ⟨downdown0|downup⟩⟨downup|downdown0⟩)))

Exp[−2 ∗ t/pulsetime]/. t* → t)//FullSimplify, t]//Expand;

f7 = −D[((((⟨downup0|updown⟩⟨updown|downup0⟩
        − ⟨downdown0|updown⟩⟨updown|downdown0⟩)))

Exp[−2 ∗ t/pulsetime]/. t* → t)//FullSimplify, t]//Expand;

f8 = −D[((((⟨downup0|downdown⟩⟨downdown|downup0⟩
        − ⟨downdown0|downdown⟩⟨downdown|downdown0⟩)))

Exp[−2 ∗ t/pulsetime]/. t* → t)//FullSimplify, t]//Expand;
```

(Take Fourier Transform of the equation 67)

```
p1=Table[f1,{t,0,pulsetime,resolution}];
p2=Table[f2,{t,0,pulsetime,resolution}];
p3=Table[f3,{t,0,pulsetime,resolution}];
p4=Table[f4,{t,0,pulsetime,resolution}];
p5=Table[f5,{t,0,pulsetime,resolution}];
p6=Table[f6,{t,0,pulsetime,resolution}];
p7=Table[f7,{t,0,pulsetime,resolution}];
p8=Table[f8,{t,0,pulsetime,resolution}];

fdif=Fourier[p1+p2+p3+p4+p5+p6+p7+p8, FourierParameters→{1,-1}];
fdif2=Table[{i/pulsetime ,Abs[fdif[[i]]]},{i,1,Length[fdif]/2}];

Bfieldplots= Plot[{{f[B][[4]] − f[B][[1]]}, {f[B][[2]] − f[B][[1]]}, {f[B][[3]] −
f[B][[2]]}, {f[B][[4]] − f[B][[3]]}}, {B, 0, MaxB}, AxesLabel →
{"B[G]", "Beatings[Hz]"}, PlotLabels → {{4 → 1}, {2 → 1}, {3 → 2}, {4 → 3}}]
```

(Give the magnetic field you want and finally plot figures)

```
Bc=0.02;
procH[Bc];Grid[{{Bfieldplots},{fourierplot}}]
```

Appendix B

The code in Mathematica that is used for calculating the Quantum beating frequencies in Deuterium as a function of magnetic field (figure 32) and the simulation of the Fourier transform of the exponential decay of the average value of the spin of electrons in z-axis due to depolarization from collisions, (figure 33).

Code

(Call the packet Quantum notation to use Dirac symbolism)
Needs ["Quantum` Notation`"];
SetQuantumAliases ;
(Defining some constants)
$Assumptions=t∈ Reals;
hbar=1.054571817*10-34;
AD= hbar* 4π *327384352.5222 /3;(Hyperfine term of D)
mb=-9.274009994*10^-24; (Bohr magneton)
me=2*mb;(Electron magnetic moment)
mnD=0.857438228*mb/1836; (Deuterium nucleus magnetic moment)
MaxB=0.1;
pulsetime=2*10^-7; (Measurement Time)
resolution=10^-10;(Time Resolution) (Defining the Hamiltonian of Hydrogen with normal magnetic field to the photodissociation axis)

HamiltonianD[B_]

$$:= \{\{A/2, aB\frac{1}{2}, 0,0,0, b\frac{B}{2}\},\{aB\frac{1}{2}, -A/2, 0,0, b\frac{B}{\sqrt{2}}, \frac{A}{\sqrt{2}}\},\{0,0, -\frac{A}{2}, aB\frac{1}{2}, A\frac{\sqrt{2}}{2}, b\frac{B}{\sqrt{2}}\},\{0,0, aB\frac{1}{2}, \frac{A}{2}, \sqrt{2}bB\frac{1}{2}, 0\},$$
$$\{0, bB\frac{1}{2}\sqrt{2}, A\frac{\sqrt{2}}{2}, bB\frac{1}{2}\sqrt{2}, 0, aB\frac{1}{2}\},\{bB\frac{1}{2}\sqrt{2}, A\frac{\sqrt{2}}{2}, bB\frac{\sqrt{2}}{2}, 0, aB\frac{1}{2}, 0\}\};$$

(Finding the eigenvalues and eigenvectors of the Hamiltonian above and sort the eigenvalues by increasing order.)

eigensys[B_]:=Eigensystem[HamiltonianH[B]/.{A→AH,a→me,b→mnH}];
esys2[B_]:= Partition[Riffle[eigensys[B][[1]],eigensys[B][[2]]],2];
esys[B_]: =Sort [Sort[esys2[B], #[[1]]<#[[2]] &]];
evals[B_]:=esys[B][[All,1]];

(Put the eigenvectors in a table and then transverse it)

ω[B_]:=1/hbar*esys[B][[All,1]];

$f[\text{B\_}]:=\frac{1}{2\pi\text{hbar}}\text{Sort}[\text{Eigenvalues}[\text{HamiltonianD}[B]/.\{A\to \text{AD}, a\to \text{me}, b\to \text{mnD}\}]];$

```
evecs[B_]:=esys[B][[All,2]];
States[B_]:=Table[evecs[B][[i]],{i,1,6}];
transstates[B_]:=Transpose[States[B]];
```

By employing the equations $|JM\rangle=\sum_{m_1m_2}C(j_1j_2;m_1m_2)|j_1m_1\rangle|j_2m_2\rangle$ or equivalently $|j_1m_1\rangle|j_2m_2\rangle=\sum_{J,M}C(j_1j_2;m_1m_2)\,|JM\rangle$ and $C(j_1j_2;m_1m_2)\equiv\langle j_1m_1j_2m_2|JM\rangle$ we express the eigenvectors for random Magnetic field as a function of $|M_S,M_I\rangle$:

$\text{procD}[\text{B\_}]:=\text{Module}[\{\text{bf}=B\},$

$\langle\psi_{\text{l}}|\psi_{\text{lpr\_}}\rangle:=\text{KroneckerDelta}[l,\text{lpr}]$

$\text{stateold}[\text{bf}]:=\text{Table}[\text{Sum}[\text{transstates}[B][[k]][[i]]|\psi_i\rangle\text{Exp}[-I\omega[\text{bf}][[i]]t],\{i,1,6\}],\{k,1,6\}];$

$\text{stateoldinit}[\text{bf}]:=\text{Table}[\text{Sum}[\text{transstates}[B][[k]][[i]]|\psi_i\rangle//\text{Chop},\{i,1,6\}],\{k,1,6\}];$

$|\text{plup0}\rangle=\text{stateoldinit}[\text{bf}][[1]]//\text{Chop};(|1\uparrow,t=0\rangle)$

$|\text{pldown0}\rangle=\text{stateoldinit}[\text{bf}][[2]]//\text{Chop};(|1\downarrow,t=0\rangle)$

$|\text{mnup0}\rangle=\text{stateoldinit}[\text{bf}][[3]]//\text{Chop};(|-1\uparrow,t=0\rangle)$

$|\text{mndown0}\rangle=\text{stateoldinit}[\text{bf}][[4]]//\text{Chop};(|-1\downarrow,t=0\rangle)$

$|\text{odown0}\rangle=\text{stateoldinit}[\text{bf}][[5]]//\text{Chop};(|0\downarrow,t=0\rangle)$

$|\text{oup0}\rangle=\text{stateoldinit}[\text{bf}][[6]]//\text{Chop};(|0\uparrow,t=0\rangle)$

$|\text{plup}\rangle=\text{stateold}[\text{bf}][[1]]//\text{Chop};(|1\uparrow,t\rangle)$

$|\text{pldown}\rangle=\text{stateold}[\text{bf}][[2]]//\text{Chop};(|1\downarrow,t\rangle)$

$|\text{mnup}\rangle=\text{stateold}[\text{bf}][[3]]//\text{Chop};(|-1\uparrow,t\rangle)$

$|\text{mndown}\rangle=\text{stateold}[\text{bf}][[4]]//\text{Chop};(|-1\downarrow,t\rangle)$

$|\text{odown}\rangle=\text{stateold}[\text{bf}][[5]]//\text{Chop};(|0\downarrow,t\rangle)$

$|\text{oup}\rangle=\text{stateold}[\text{bf}][[6]]//\text{Chop};(|0\uparrow,t\rangle)$

(Employing equation 75)

$\text{a1}=D[\langle\text{plup0}/\text{plup}\rangle\langle\text{plup}/\text{plup0}\rangle$
$-\langle\text{pldown0}/\text{plup}\rangle\langle\text{plup}/\text{pldown0}\rangle//\text{FullSimplify},t]//\text{Expand};$

$\text{a2}=-D[\langle\text{plup0}/\text{pldown}\rangle\langle\text{pldown}/\text{plup0}\rangle$
$-\langle\text{pldown0}/\text{pldown}\rangle\langle\text{pldown}/\text{pldown0}\rangle//\text{FullSimplify},t]//\text{Expand}$

$\text{a3}=D[\langle\text{plup0}/\text{oup}\rangle\langle\text{oup}/\text{plup0}\rangle-\langle\text{pldown0}/\text{oup}\rangle\langle\text{oup}/\text{pldown0}\rangle//\text{FullSimplify},t]//\text{Expand}$

$$a4 = -D[\langle plup0/odown\rangle\langle odown/plup0\rangle - \langle pldown0/odown\rangle\langle odown/pldown0\rangle//FullSimplify, t]//Expand$$

$$a5 = D[\langle plup0/mnup\rangle\langle mnup/plup0\rangle - \langle pldown0/mnup\rangle\langle mnup/pldown0\rangle//FullSimplify, t]//Expand;$$

$$a6 = -D[\langle plup0/mndown\rangle\langle mndown/plup0\rangle - \langle pldown0/mndown\rangle\langle mndown/pldown0\rangle//FullSimplify, t]//Expand;$$

$$a7 = D[\langle oup0/plup\rangle\langle plup/oup0\rangle - \langle odown0/plup\rangle\langle plup/odown0\rangle//FullSimplify, t]//Expand;$$

$$a8 = -D[\langle oup0/pldown\rangle\langle pldown/oup0\rangle - \langle odown0/pldown\rangle\langle pldown/odown0\rangle//FullSimplify, t]//Expand;$$

$$a9 = D[\langle oup0/oup\rangle\langle oup/oup0\rangle - \langle odown0/oup\rangle\langle oup/odown0\rangle//FullSimplify, t]//Expand;$$

$$a10 = -D[\langle oup0/odown\rangle\langle odown/oup0\rangle - \langle odown0/odown\rangle\langle odown/odown0\rangle//FullSimplify, t]//Expand;$$

$$a11 = D[\langle oup0/mnup\rangle\langle mnup/oup0\rangle - \langle odown0/mnup\rangle\langle mnup/odown0\rangle//FullSimplify, t]//Expand;$$

$$a12 = -D[\langle oup0/mndown\rangle\langle mndown/oup0\rangle - \langle odown0/mndown\rangle\langle mndown/odown0\rangle//FullSimplify, t]//Expand;$$

$$a13 = D[\langle mnup0/plup\rangle\langle plup/mnup0\rangle - \langle mndown0/plup\rangle\langle plup/mndown0\rangle//FullSimplify, t]//Expand;$$

$$a14 = -D[\langle mnup0/pldown\rangle\langle pldown/mnup0\rangle - \langle mndown0/pldown\rangle\langle pldown/mndown0\rangle//FullSimplify, t]//Expand;$$

$$a15 = D[\langle mnup0/oup\rangle\langle oup/mnup0\rangle - \langle mndown0/oup\rangle\langle oup/mndown0\rangle//FullSimplify, t]//Expand;$$

$$a16 = -D[\langle mnup0/odown\rangle\langle odown/mnup0\rangle - \langle mndown0/odown\rangle\langle odown/mndown0\rangle//FullSimplify, t]//Expand;$$

$$a17 = D[\langle mnup0/mnup\rangle\langle mnup/mnup0\rangle - \langle mndown0/mnup\rangle\langle mnup/mndown0\rangle//FullSimplify, t]//Expand;$$

$$a18 = -D[\langle mnup0/mndown\rangle\langle mndown/mnup0\rangle - \langle mndown0/mndown\rangle\langle mndown/mndown0\rangle//FullSimplify, t]//Expand;$$

(Take Fourier Transform of the equation 67)

```
r1=Table[a1,{t,0,pulsetime,resolution}];
r2=Table[a2,{t,0,pulsetime,resolution}];
r3=Table[a3,{t,0,pulsetime,resolution}];
r4=Table[a4,{t,0,pulsetime,resolution}];
r5=Table[a5,{t,0,pulsetime,resolution}];
r6=Table[a6,{t,0,pulsetime,resolution}];
r7=Table[a7,{t,0,pulsetime,resolution}];
```

```
r8=Table[a8,{t,0,pulsetime,resolution}];
r9=Table[a9,{t,0,pulsetime,resolution}];
r10=Table[a10,{t,0,pulsetime,resolution}];
r11=Table[a11,{t,0,pulsetime,resolution}];
r12=Table[a12,{t,0,pulsetime,resolution}];
r13=Table[a13,{t,0,pulsetime,resolution}];
r14=Table[a14,{t,0,pulsetime,resolution}];
r15=Table[a15,{t,0,pulsetime,resolution}];
r16=Table[a16,{t,0,pulsetime,resolution}];
r17=Table[a17,{t,0,pulsetime,resolution}];
r18=Table[a18,{t,0,pulsetime,resolution}];
fdif = Fourier[(r1 + r2 + r3 + r4 + r5 + r6 + r7 + r8 + r9 + r10 + r11 + r12 + r13 + r14
                + r15 + r16 + r17 + r18), FourierParameters → {1, −1}];

fdif2=Table[{i/pulsetime ,Abs[fdif[[i]]]},{i,1,Length[fdif]/2}];

Bfieldplots= ListLinePlot[{f[B][[2]] − f[B][[1]], f[B][[3]] − f[B][[2]], f[B][[4]] −
f[B][[3]], f[B][[5]] − f[B][[4]], f[B][[6]] − f[B][[5]], f[B][[6]] − f[B][[1]], f[B][[5]] −
f[B][[2]], f[B][[4]] − f[B][[1]]}, AxesLabel → {"B[G]", "Beatings[Hz]"}, PlotLabels → {{2 →
1}, {3 → 2}, {4 → 3}, {5 → 4}, {6 → 5}, {6 → 1}, {5 → 2}, {4 → 1}}]
```

(Give the magnetic field you want and finally plot figures)

```
Bc=0.02;
procD[Bc];Grid[{{Bfieldplots},{fourierplot}}]
```

References

[1] E. Hecht, *fifth edition 5 Optics*. .

[2] B. P. N. Schatz, “The Faraday Effect,” vol. IV, 1933.

[3] *chiral analysis*. .

[4] A. S. Laporte and P. A. Moldauer, “Optics : Vol . 5 of Lectures on Theoretical Physics,” vol. 5, 1955.

[5] F. Rotation, “Derivation of Faraday Rotation,” no. 3, pp. 1–4.

[6] L. Bougas *et al.*, “Chiral cavity ring down polarimetry : Chirality and magnetometry measurements using signal reversals Chiral cavity ring down polarimetry : Chirality and magnetometry measurements using signal reversals,” vol. 104202, 2015.

[7] P. M. Biot, “ment à leur surface, j’ai été conduit à la dé-,” no. i.

[8] M. Vallet, F. Bretenaker, A. Le Floch, and J. The, “Resonant Cavity Gas-Phase Polarimeter,” vol. 70, no. 21, pp. 4636–4639, 1998.

[9] D. Jacob, F. Bretenaker, P. Pourcelot, P. Rio, M. Dumont, and A. Dore, “Pulsed measurement of high-reflectivity mirror phase retardances,” vol. 33, no. 15, pp. 3175–3178, 1994.

[10] D. Sofikitis, L. Bougas, G. E. Katsoprinakis, A. K. Spiliotis, B. Loppinet, and T. P. Rakitzis, “Evanescent-wave and ambient chiral sensing by signal-reversing cavity ringdown polarimetry,” *Nature*, vol. 514, no. 7520, pp. 76–79, 2014.

[11] D. Sofikitis *et al.*, “Microsecond-resolved SDR-based cavity ring down ellipsometry,” vol. 54, no. 18, 2015.

[12] B. Jirgensons, “Optical Rotation and Viscosity of Native and Denatured Proteins . II . Influence of Temperature and Concentration ’,” 1952.

[13] H. Denaturation, C. N. Pace, and T. Mcgrath, “Substrate Stabilization of Lysozyme to Thermal and Guanidine [a,” no. 15, pp. 3862–3865, 1979.

[14] A. Gordon, “Optical Rotatory Dispersion Including & hymotrypsin Studies of Globular Proteins ,” vol. 243, pp. 4615–4626, 1968.

[15] J. P. Halper, N. Latovitzki, H. Bernstein, and S. Beychokt, “Optical Activity of Human Lysozyme,” vol. 68, no. 3, pp. 517–522, 1971.

[16] ALBERT A. MICHELSON and EDWARD W. MORLEY, “On a method of making the wavelength of sodium light the actual and practical standard of length,” pp. 427–430, 1887.

[17] “Jackson J D Classical Electrodynamics (Wiley, 1962)(T)(656S).pdf.” .

[18] A. P. A. M. Dirac, “The Quantum Theory of the Electron The Quantum Theory of the Electron .,” vol. 117, no. 778, pp. 610–624, 2013.

[19] Zare, *Angular Momentum*. .

[20] Foot, “Atomic and molecular physics.”

[21] Griffiths, *introduction to Eletrodynamics*. .

[22] H. Zheng *et al.*, “Microwave-free vector magnetometry with nitrogen-vacancy centers along a single axis in diamond,” pp. 1–9.

[23] A. You, M. A. Y. Be, and I. In, “Time-resolved surface magnetometry in the nanosecond scale using synchrotron radiation,” vol. 1563, no. October 1997, 1998.

[24] A. Phys, “Ultrafast pulsed magnetic fields generated by a femtosecond laser,” vol. 072405, no. April, pp. 1–5, 2018.

[25] A. K. Spiliotis, M. Xygkis, M. Koutrakis, K. Tazes, and G. K. Boulogiannis, “Ultrahigh-Density Spin-Polarized Hydrogen Isotopes from the Photodissociation of Hydrogen Halides : New Applications for Laser-Ion Acceleration , Magnetometry , and Polarized Nuclear Fusion.”

[26] D. Sofikitis, C. S. Kannis, G. K. Boulogiannis, and T. P. Rakitzis, “Ultrahigh-Density Spin-Polarized H and D Observed via Magnetization Quantum Beats,” *Phys. Rev. Lett.*, vol. 121, no. 8, p. 83001, 2018.